HYDROLOGIC CONTROLS ON REMOVAL OF OXYGEN IN THE BED OF A MOUNTAIN STREAM, EAST RIVER, COLORADO

by

Erin M. Cantrell

B.S., Cornell University, 2017

A thesis submitted to the

Faculty of the Graduate School of the

University of Colorado in partial fulfillment

of the requirement for the degree of

Master of Science

Department of Environmental Engineering

2020

Committee Members:

Michael Gooseff

Katherine Lininger

Diane McKnight

Abstract:

Cantrell, Erin M. (M.S., Environmental Engineering)

Hydrologic Controls on Removal of Oxygen in the Bed of a Mountain Stream, East River, Colorado

Thesis directed by Professor Michael Gooseff

Dissolved oxygen (DO) concentrations in rivers are critical for aquatic habitat and controlled by biological generation and uptake, and physical factors. One important physical factor is hydrology: not only streamflow dynamics (changing amounts of water), but also changes in surface-groundwater exchanges. Over a period of 15 months in East River, Colorado from August 2017 (a somewhat 'average' flow year) to October 2018 (a low flow year) high frequency (5 minute) DO and temperature data were collected in the water column of the river and directly in the streambed at depths of 10 cm, 20 cm, and 35 cm. Using the VFLUX2 model, temperature data were used to estimate vertical upwelling and downwelling vertical fluxes of water (and solutes). We find that there was downwelling throughout both years, and increased fluxes into the bed during peak flows. From relating vertical flux to steam discharge and groundwater tables we find that stream discharge is a control of streambed DO during low flow. We calculated DO removal from the channel into the bed, finding enhanced removal rates in 2018 compared to 2017. We observed an extended hyporheic anoxic period throughout the summer and fall of 2018 due to the increased DO removal rates within the hyporheic zone. The three subsurface locations were found to not all be on the same flow path, which may account for some non-linear DO concentration decreases with depth in 2017. Anoxia (zero DO concentration) is observed briefly in 2017 and for an extended period in 2018. Increased DO removal due to low flow conditions and increased temperature are the primary factors for anoxia in 2018. The anoxia patterns differ between the two years, so it is likely that the cause of anoxia differs. To better understand the system dynamics, three periods of atypical DO or vertical flux were analyzed as more detailed small events. These helped us to understand system storm responses and causes of anoxia. This research has advanced our understanding of the dependence of DO in both the streambed and open channel on stream-groundwater exchanges by showing periods of stream discharge control on DO dynamics and increased DO removal at low flow and high temperature.

Acknowledgements:

This material is based upon work supported by OptioO2, CU Graduate School, the US Dept. of Energy (DOE), Office of Science, Small Business Initiative Research, under award number DE-SC0017129 Program manager: Paul Bayer. This material is partially based upon work supported through the Lawrence Berkeley National Laboratory's Watershed Function Scientific Focus Area. The DOE Office of Biological and Environmental Research funded the work under contract DE-AC02-05CH11231, DOE grant DE-SC0018165. Special thanks to Michael Wilkins, Marty Briggs, and Scott Wieland for their help with this project.

Contents:

List of Tables:

List of Figures:

Introduction:

In streams, dissolved oxygen (DO) is controlled by both biological factors and physical factors. One of the most important of the physical factors that influences dissolved oxygen dynamics in streams is hydrology: not only streamflow state and changes, but also changes in surface-groundwater exchanges. DO is largely controlled by primary production by autotrophs, exchange with the atmosphere, water temperature, and consumption by heterotrophic organisms (e.g. fish spawning, bacterial activity, and macroinvertebrates). Many heterotrophic microorganisms live in riverbeds consuming oxygen and organic matter, therefore microbial activity is an important component of the stream ecosystem.

Stream and streambed DO are vital for aquatic life. Low DO conditions can lead to many harmful outcomes for fish, especially salmonid species that rely heavily on cold water and high DO streams. Fish redds depend on elevated DO concentrations to survive incubation in riverbed sediments. Periods of strong groundwater influence from upwelling can lead to low DO and have been shown to kill whole redds (Malcolm et al., 2004). On the other hand, groundwater is vital in the summer to keeping the stream temperatures low enough to be habitable by salmonids and other cold water fish (Larson and Woelfle-Erskine, 2018). Salmonid redds are seen in areas of regional upwelling in that reach, but local downwelling at the redd site (Baxter and Hauer, 2000) to balance these two factors.

Hyporheic zones are areas were groundwater and surface water meet in sediments adjacent to and underneath streams. Hyporheic dynamics are established by catchment geology and modified by stream discharge rates, which affect sediment distribution (Valett et al., 1997). If this sediment distribution is heterogeneous, it can cause increased depth of hyporheic mixing and changes in water residence time in the hyporheic zone (Sawyer and Cardenas, 2009). These hyporheic dynamics can have large impacts on DO fluxes into the streambed and stream chemistry (Findlay, 1995) including residence time and microbial activity affecting DO removal rates. When the hyporheic zone is included in stream

DO assessments, this can considerably alter the balance of the stream DO producers and consumers (Grimm and Fisher 1984). The physical processes in the hyporheic zone can have far reaching impacts on the DO dynamics of a stream and their impacts on biota. Increased stream flow and therefore increased vertical flux can lead to higher levels of DO (Malcolm et al., 2004) as higher DO stream water, which has mixed with the atmosphere, is pushed into the subsurface. Generally, the higher stream flow times are characterized by higher hyporheic DO, while low flow has lower hyporheic DO (Malcolm et al., 2004).

In this study, we seek to evaluate the dynamic of downwelling/upwelling across the ice-free season in a subalpine river and the coincident changes in DO through the streambed. Novel DO optodes were deployed for over 14 months (July 2017 to October 2018) in the East River, Colorado in the river water column and in the streambed at depths of 10, 20, and 35 cm. These years represent, respectively, a typical flow year and a low flow year. High frequency (5 min interval) data from these sensors provide an unprecedented view of coupled stream-groundwater exchanges and benthic biological processes over these two vastly different summer flow regimes. We use the VFLUX2 model to estimate time series of vertical fluxes during the ice-free season and then calculate changes in DO from one location to the next based on these flux values and DO measurements at the surface and in the subsurface. To further explore these various factors and their influence on DO, correlations of the daily averaged data will explore how the different factors like DO, stream discharge, groundwater elevation, vertical flux (VFLUX) and change in DO concentration (ΔDO) interact and if there are any relationships showing when certain factor control DO. We expect there to be more control on DO dynamics and generally lower DO at low stream discharge. In addition, we expect increased microbial activity in 2018 due to both low flow and increased temperatures. This increased microbial activity will lead to increased DO removal and lower DO concentrations in the streambed.

Site Description:

East River is a 300-km^2 mountainous headwater alluvial stream in the Upper Colorado Basin. It is located in the Rocky Mountains of Colorado near Crested Butte and has an average elevation of 3266m with 1420m of topographic relief (Hubbard et al. 2018). The study site was located in a riffle near the head of a meander bend at the bottom of a Lower Montane hillslope. It was 120 m downstream of the pumphouse discharge measuring station (Figure 1). At this measuring station continuous data is collected by the Lawrence Berkeley National Laboratory on stream stage (which is converted to discharge from field measurements of discharge and generation of a rating curve) and meteorological data. Water table elevation was measured daily at the PLM6 well, which is near the base of sloping valley wall to the south of the East River (Tokunaga et al., 2019, Figure 1). Stream discharge is measured at a ten-minute interval just downstream of a Pumphouse used to extract water for municipal demand (Carrol and Williams, 2019). The study site is part of the designated headwater mountainous watershed testbed led by Lawrence Berkley Nation Laboratory and supported by US Department of Energy (DOE) Biological and Environmental Research Subsurface Biogeochemistry Program (Hubbard et al., 2018).

The study site has characteristic long cold winters and shorter summers, with much of the streamflow dominated by snowmelt in the spring and summer. The watershed has a mean annual temperature of ~0 °C (Hubbard et al., 2018). On average the watershed receives 1200 mm/year of precipitation (PRISM Climate Group, 2015) most of which is snow. The area is continental, with a subarctic climate, and hosts montane, subalpine, and alpine ecosystems (Hubbard et al., 2018). The streambed primarily consists of cobbles, gravel, and sand underlain by Cretaceous Mancos shale (Nelson et al., 2019). Land use in the watershed is like other alpine Colorado areas with skiing and tourism being the main uses but also having significant uses for ranching and mining.

Figure 1: (top) Aerial view of the field site with pumphouse, PLM6, and sensors locations labeled. (bottom) Field photo looking across the valley.

Methods

VFLUX methods

OptiO2 sensors provided temporally (Δt = 5min) resolved measurements of DO and temperature from the river and three probes buried directly in the sediment at 10 cm, 20 cm, and 35 cm. I refer to the subsurface layers bounded by the sensor layout as "r-10", "10-20", and "20-35" in some places in this thesis. Continuous measurements were made over 14 months including over winter freeze-in. We used these high frequency, long term temperature measurements to estimate streambed vertical water flux with the VFLUX2 numerical model (Irvine et al., 2015 and Gordon et al., 2012). Direct flux measurements are difficult to make especially over extended periods of time at high frequencies. Flux estimates from heat transport equations have been shown to have less error than estimates from Darcy's equation alone mainly due to spatial heterogeneity and issues effectively measuring hydraulic conductivity (Lautz, 2010), for these reasons we used the VFLUX2 model. VFLUX2 models 1-D vertical flux of heat using a generalized heat transport equation to simulate streambed temperatures:

$$\frac{\partial T}{\partial t} = \kappa_e \frac{\partial^2 T}{\partial z^2} - \frac{v}{\gamma}\frac{\partial T}{\partial z}$$

Where T is temperature (^{o}C), t is time (s), κ_e is effective thermal diffusivity ($m^2\ s^{-1}$), z is depth (m), *v* is vertical seepage flux ($m\ s^{-1}$), *γ* is the ratio of the heat capacity of the streambed sediment-water matrix to the heat capacity water. The fundamental heat transport equation can be solved through several options in VFLUX2. Because we had specific sediment thermodynamic properties as reporded by Bryant et al. (2020), we chose to use the amplitude ratio method (HatchAr) that was pioneered by Hatch et al. (2006).

The advection term from these simulations is used to inform the groundwater flux from streambed temperatures based on one of six chosen approaches to simulating heat transfer in the bed, then filters data based on sinusoidal temperature fluctuations using a Dynamic Harmonic Regression

(DHR) (Taylor et al., 2007, Young et al., 1999). The model assumes periodic, sinusoidal temperature oscillations, purely 1-D flow, steady-state condition of magnitude of flux (Stallman, 1965, Keery et al., 2007), and no thermal gradient with depth in the streambed (i.e., the SW-GW boundary temperature is the average stream temperature). These assumptions do not all have to be met to have valid model results. For example, the presence of a thermal gradient has been shown to not generate large estimation errors and non-sinusoidal stream temperatures, when filtered, produce values within 10% of the true value (based on laboratory experiments in Lautz, 2010). Raw temperatures are filtered with DHR because they are not purely sinusoidal and are used to isolate the periodic temperature signal of interest prior to deriving the changing amplitude and phase of the signal (Lautz, 2012). VFLUX can be considered a transient model when used with field data (Jensen and Engesgaard, 2011; Rau et al., 2010) as a single point in time is based on an assumption that flux is unchanging but is then strung together as a series of these single points to create a dynamic set of flux estimates over time (Lautz, 2012).

The HatchAr solution to the heat transport equation has been shown to be more accurate than methods using lag time especially in field studies with non-ideal conditions and well-known bed characteristics and is the recommended method (Lautz, 2010, Briggs et al., 2014). This method uses the following equations to calculate a ratio of temperature amplitudes over time to use heat as a conservative tracer for water movement. The altitude ratio (Ar) is calcuated as :

$$A_r = \exp\left\{\frac{\Delta z}{2\kappa_e}\left(v - \sqrt{\frac{\alpha + v^2}{2}}\right)\right\}$$

where Δz is the sensor spacing, v is the rate of penetration of the thermal front, which is proportional to the fluid velocity: $v = v_f/\lambda$. Where, v_f is the fluid velocity and λ is the thermal conductivity

$$\alpha = \sqrt{v^4 + (\frac{8\pi\kappa_e}{P})^2}$$

where P is temperature variations = 1/frequency (Hatch et al., 2006)

In HatchAr, thermal diffusivity is represented as:

$$\kappa_e = \frac{\lambda_e}{\rho c} = \frac{\lambda_0}{\rho c} + \beta|v_f|$$

where, λ_e is the effective thermal conductivity, λ_0 is the baseline thermal conductivity (in the absence of fluid flow), and β is thermal dispersivity (Ingebritsen and Sanford, 1998).

VFLUX2 uses thermal diffusivity values to solve the heat transfer equation and estimate the vertical flux within the bed. In the HatchAr method, thermal diffusivity is based on physical sediment and water column parameters which are input for the site being modeled. The values used for our model (Table 1) are based on values from Bryant et al. (2020) where extensive characterization of the sediment was done in the same area as our probe deployment.

Table 1: VFLUX Parameters used for model calibration.

Parameter	**Variable**	**Value**	**Confidence Interval**	**Units**
Porosity	n	0.27	0.027	N/A
Thermal conductivity	K_{cal}	0.00444	0.000006381	cal/s cm °C
Volumetric heat capacity of sediment	C_{scal}	0.447	0.00779	cal/ cm^3 °C
Volumetric heat capacity of water	C_{wcal}	1	0.00120	cal/cm^3 °C
Dispersivity	β	0.01	0.0075	m

In using the HatchAr model, we can evaluate the daily amplitudes of observed temperature timeseries and the associated amplitude ratios, Ar, (deep sensor amplitude / shallow sensor amplitude) between two temperature sensors shown in the Amplitude ratio equation above. These Ar values should not be close to zero, and they should not be close to or greater than one (Lautz, 2012). From our VFLUX modeling, we have identified an upper Ar limit of 0.83. Strong departures in the Ar timeseries were considered to be suspect. From this criterion a problem period from August 3, 2018 to the end of the period in October 2018 from the riverbed to 10 cm depth was identified and removed. This shift in Ar occurs because the 10 cm diurnal temperature signal is larger than the river temperature signal causing problematically large amplitude ratios.

Process Foci

We carefully examined the raw temperature on a daily basis to determine where subsurface thermal gradients changed abruptly, and where daily sinusoidal patterns were dampened and/or the temporal pattern was not enough of a clear sinusoid even with DHR filtration. During these times, estimated fluxes would change abruptly relative to other times and/or fall outside of theoretical bounds. These instances forced further examination of the raw temperature, raw atmospheric data, and estimated fluxes. When rapid changes in field conditions and system dynamics were found, they were examined with special attention with zoom-ins on short time periods as will be shown later in this thesis. For example on Sept 23 and 24, 2017 cold air temperatures change the river temperature daily sinusoid, which affects estimated fluxes in river to 10 cm depth causing a spike in the flux value, but we decided to keep these flux estimates as valid because they do not fall outside theoretical bounds and likely indicate true phenomena for example due to changes in water viscosity with temperature (Cozzetto et al. 2013).

Based on the criteria listed previously, the VFLUX2 model run for the dates in Table 1 are considered valid and will be used in the subsequent section of the thesis. The period from October 29, 2017 to April 23, 2018 was excluded from the VFLUX2 model due to dampening of the temperature to non-sinusoidal patterns during winter and stream freeze.

Table 2: The dates listed above are the continuous time period when VFLUX modeling is considered to be valid. 00:00 is considered to be the start of the day listed (i.e. midnight).

Hatch Flux$_{r\text{-}10}$

Start Date	End Date
7/31/2017 12:10	10/29/2017 00:00
4/23/2018 00:00	8/3/2018 00:00

Hatch Flux$_{10\text{-}20}$

Start Date	End Date
7/31/2017 12:10	10/29/2017 00:00
4/23/2018 00:00	10/5/2018 13:45

Hatch Flux$_{20\text{-}35}$

Start Date	End Date
7/31/2017 12:10	10/29/2017 00:00
4/23/2018 00:00	10/5/2018 13:45

Calculating the change of dissolved oxygen concentrations

To relate the change in DO concentration (ΔDO) and hydrologic parameters, VFLUX2 flux estimates were used to estimate the amount of DO gained or removed between each sensor as the water moved into the streambed. This was accomplished using the VFLUX2 velocity measurements at time *t* to calculate how long the water would have taken to travel the 10 cm or 15 cm distance between the sensors.

$$t - \tau = \Delta z / v(t)$$

where, *v*(t) = calculated flux (from VFLUX) from between two paired sensors depths at time *t* (LT^{-1}) and Δz = sensor spacing. To calculate $\Delta DO(t)$ we start with the $DO_x(t)$and for each data point, find the corresponding *v*(t). Then calculate τ by rearranging for: $\tau = t - \frac{\Delta z}{v(t)}$. Now, with τ, we find $DO_{x-1}(\tau)$ and take the difference of $DO_x(t)$ from it. The full equation along with a conceptual diagram are shown below (Figure 2).

$$\Delta DO = DO(t - \tau) - DO_x(t)$$

where DO = concentration of dissolved oxygen where subscripts denote depth of observation, t = time at which DO was observed at a set depth (i.e. 10 cm), τ = time at which stream water is predicted to have begun to infiltrate into the bed, x = starting DO sensor (e.g. 10cm), and x-1 = back paired sensor (e.g. river).

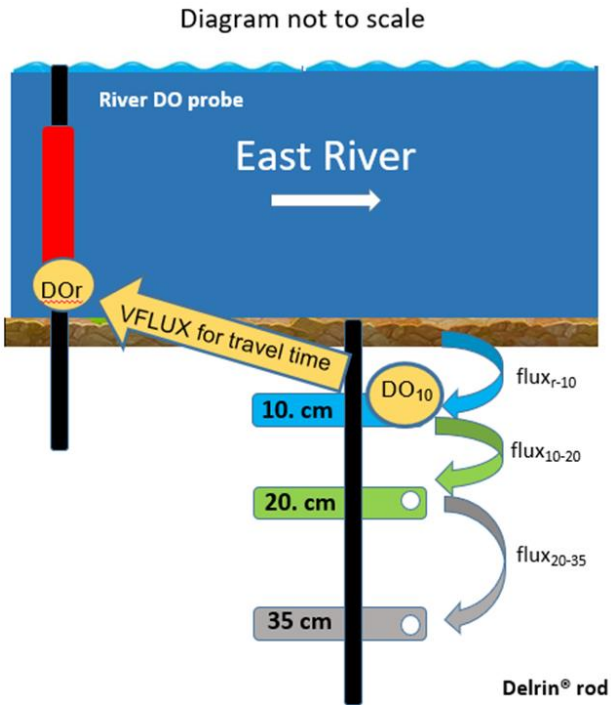

Figure 2: A theoretical diagram showing how ΔDO is calculated. Sensor spacing, modeled vertical fluxes and their use in back pairing DO are shown.

Values of *ΔDO* are considered valid for the times where VFLUX2 is considered valid. However, the Δ*DO* estimates begin a few hours after the start of the 2017 sampling period to account for travel times that would start at the time of data collection initiation. A stipulation was added that limits the amount of time needed to travel between the paired sensors to three days though travel times exceeding three days have been reported in heterogenous beds in other rivers (Sawyer and Cardenas, 2009) . If travel times exceeded this three day limit then they were omitted from the *ΔDO* data series. There are also locations in the data that show a zero value which is an instance when the initial and receiving layers both have the same DO concentration value which happens in the 10 cm to 20 cm and 20 cm to 35cm layers in 2018 due to the extended anoxic period in the bed. We also calculated the proportional change in ΔDO as $\frac{\Delta DO}{DO_{x-1}}$.

Results:

General Results:

The reduction in snowpack that was observed in the 2017-2018 winter is apparent from observation of both the time series of river flows and water table elevations in 2018 compared to those in 2017 (Figure 3B) and the monthly mean discharge (Table 3). The groundwater elevation is always higher in 2017 than 2018 at the same time of year (Table 4) and the river discharge is almost always higher at the same time of year, though only 10 months were on reported not the full twelve. The 2017 January to October mean discharge is 2.71 cms while the 2018 January to October mean discharge is 1.22 cms. November and December 2017 were excluded to keep the averaged time periods the same between the two years as there is not data for November and December 2018.

Table 3: Mean monthly discharge (cms)

Month	2017	2018
January	0.36	0.33
February	0.34	0.33
March	0.76	0.33
April	2.10	1.30
May	5.28	4.35
June	11.73	2.78
July	3.65	0.93
August	1.38	0.55
September	0.79	0.45
October	0.72	0.82
November	0.61	
December	0.40	

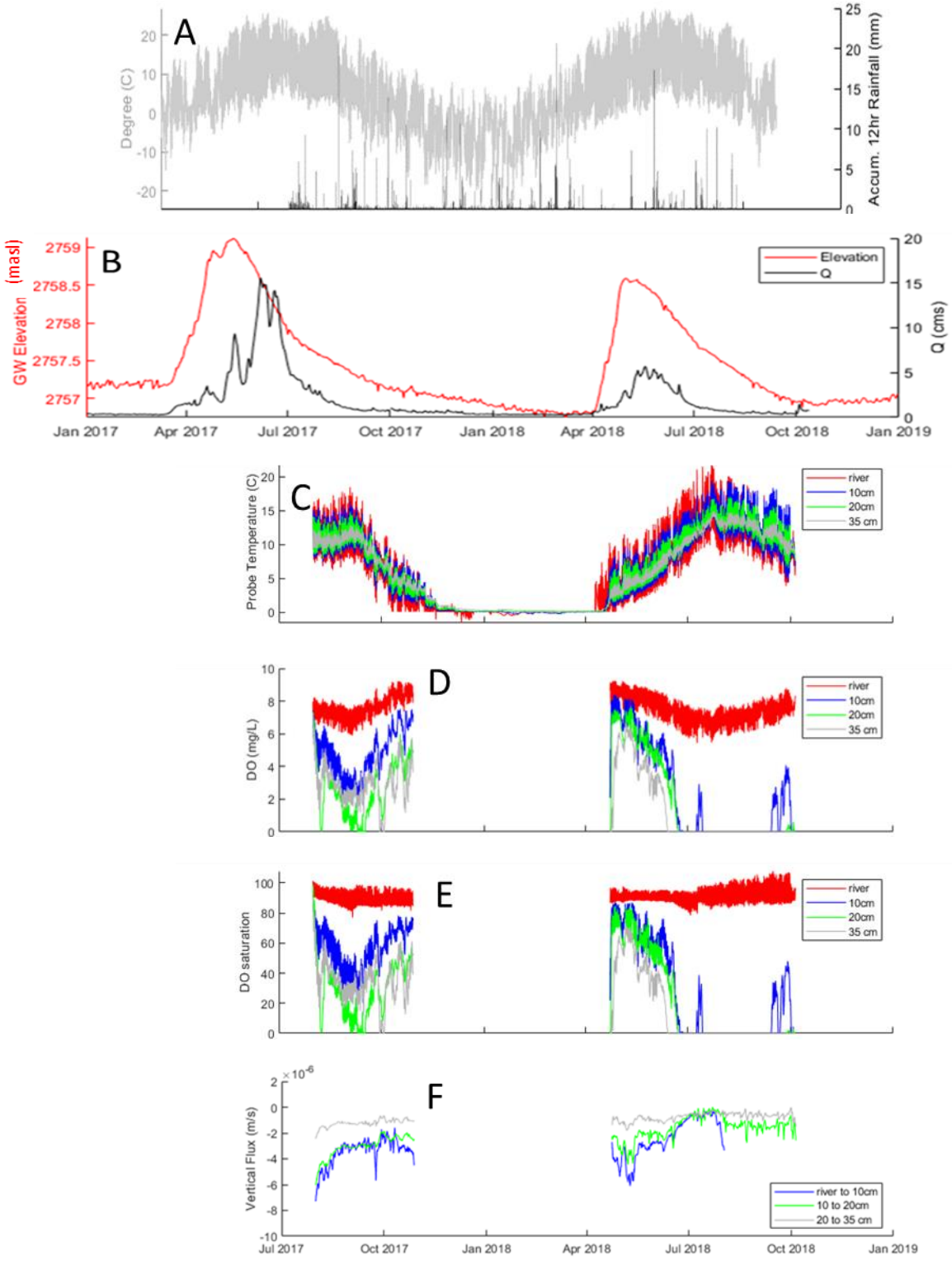

Figure 3: The time series shows the measured (A-D) and modeled (F) data where A) is air temperature and the 12-hr accumulated rainfall. B) is stream discharge from the pumphouse gauge and groundwater elevation from PLM6. (C- E) show the measured temperature, DO concentration, and DO saturation and

each depth over the modeled period. F) show the VFLUX model estimated velocity with negative being a downward flux into the sediment. Note the x-axes span different time lengths but are lined up for dates to match.

Table 4: PLM6 Monthly mean groundwater elevation above sea level (masl)

Month	2017	2018
January	2757.18	2756.88
February	2757.20	2756.83
March	2757.29	2756.80
April	2758.38	2757.65
May	2758.97	2758.48
June	2758.33	2758.03
July	2757.71	2757.59
August	2757.44	2757.29
September	2757.21	2757.04
October	2757.10	2756.94
November	2757.03	2756.96
December	2756.96	2756.99

Not only was 2018 a dryer year than 2017 (Table 5), but it was also a warmer year on average. August, September, and October had much warmer stream temperatures in 2018 than 2017 (Table 6) which points to higher air temperatures. These months are important months for evaporation, with higher air temperatures there could be more evaporation which would exacerbate the already lower water level. Stream temperatures range from 14.11 to 2.02°C with July 2017 being the warmest month and April 2018 being the coldest at all depths (Table 6). The higher average temperatures in 2018 compared to 2017 at all depths in the streambed may lead to increased microbial activity and related oxygen removal in the subsurface in 2018 compared to 2017. There is also higher temperature in the streambed compared to the river in August to October 2018 (Table 6) which caused the previously mentioned issues with VFLUX from river to 10 cm depth during this period.

Table 5: Monthly mean 12-hr accumulated rainfall, (mm)

Month	2017	2018
April		1.15
May		0.19
June		0.33
July	0.85	0.89
August	0.94	0.73
September	1.13	0.64
October	0.92	
November	0.64	
December	0.56	

Table 6: Monthly mean sensor temperature (°C) for the modeled time

	River	10 cm	20 cm	35 cm
Jul-2017	14.11	13.52	12.73	11.15
Aug-2017	11.26	11.23	11.09	10.70
Sep-2017	9.57	9.92	9.94	9.91
Oct-2017	3.89	4.62	4.79	5.14
Apr-2018	2.02	1.32	1.19	1.15
May-2018	5.21	5.11	4.98	4.67
Jun-2018	9.58	9.33	8.99	8.41
Jul-2018	13.94	13.80	13.30	12.58
Aug-2018	13.52	13.99	13.77	13.31
Sep-2018	10.60	11.43	11.38	11.24
Oct-2018	8.23	8.78	9.03	9.28

Though stream DO stays relatively constant between the two years, the subsurface has an extended anoxic period from July to October of 2018 (Table 7, Figure 3D and 3E). The stream even has higher DO saturation during September and October period in 2018 than it did in 2017 with 93.09% and 91.09% compared to 88.06% and 86.15% (Table 7). From Figure 3D, we can see that both years have period of anoxia at depth, but the dynamics and length of this anoxia vary vastly between the two years. Even when looking at DO saturation (Figure 3E), which takes temperature into account, these anoxia dynamics do not seem to change from the patterns seen in the concentration.

Table 7: Monthly mean DO concentration and saturation

	DO (mg/L)				DO saturation (%)			
	River	10cm	20cm	35cm	River	10cm	20cm	35cm
Jul-2017	7.13	6.34	7.18	6.79	95.77	83.85	93.61	85.17
Aug-2017	7.19	4.44	2.54	3.15	90.50	55.83	31.91	39.14
Sep-2017	7.27	3.66	1.22	2.59	88.28	44.52	14.62	31.71
Oct-2017	8.34	6.23	3.95	3.26	88.06	66.91	42.41	35.32
Apr-2018	7.49	2.07	1.85	3.75	76.25	21.66	19.34	36.86
May-2018	8.27	6.37	5.96	4.67	90.44	69.54	65.00	50.42
Jun-2018	7.38	3.04	2.40	1.02	89.50	36.09	28.18	11.62
Jul-2018	6.69	0.23	0.00	0.00	89.35	3.02	0.00	0.00
Aug-2018	6.90	0.00	0.00	0.00	91.74	0.00	0.00	0.00
Sep-2018	7.47	1.16	0.03	0.00	93.09	14.45	0.13	0.00
Oct-2018	7.71	0.25	0.09	0.00	91.09	3.03	0.45	0.00

Correlations:

The VFLUX model results show that the water in the river is downwelling over the entire modeled period in July to October 2017 and April to October 2018 (Figure 3F). The flux estimates are generally higher at times when the river flow is higher, but fluxes also spike when there are large rain events (like mid-September 2018 which will be discussed more in a later section of the results). The river to 10cm flux shows the most variability due to the more dynamic conditions in the river from environmental influences like storms and temperature changes.

Increased stream discharge is expected to drive more exchange through the bed with some seasonal hysteresis due to snowmelt impacts on stream discharge. In Figure 4A, the VFLUX and Q relationship shows a linear pattern in 2017 with the slope decreasing with depth in the 10cm to 20cm depth flux and the 20cm to 35cm depth flux (Figure4B and C) which meets expectations along with the scattering of points in October being more condensed and linear with depth which may indicate an incomplete hysteresis relationship. 2018 relationships in the fluxes at all layers (Figures 4D-F) show

hysteresis loop patterns that become more vertically close as the depth increases from river to 10 cm depth being the broadest VFLUX range (Figure 4D) 20 cm to 35cm depth being the narrowest VFLUX range (Figure 4F). This is similar to our expectation with increasing flux with increasing discharge during snowmelt and decreasing flux with decreasing discharge during the snowmelt recession. In 2017, the pattern may have also been hysteretic if an earlier time period was recorded due to the ramp up to peak then dip of river discharge during snowmelt, but this hydrologic change occurred before the sensors were deployed.

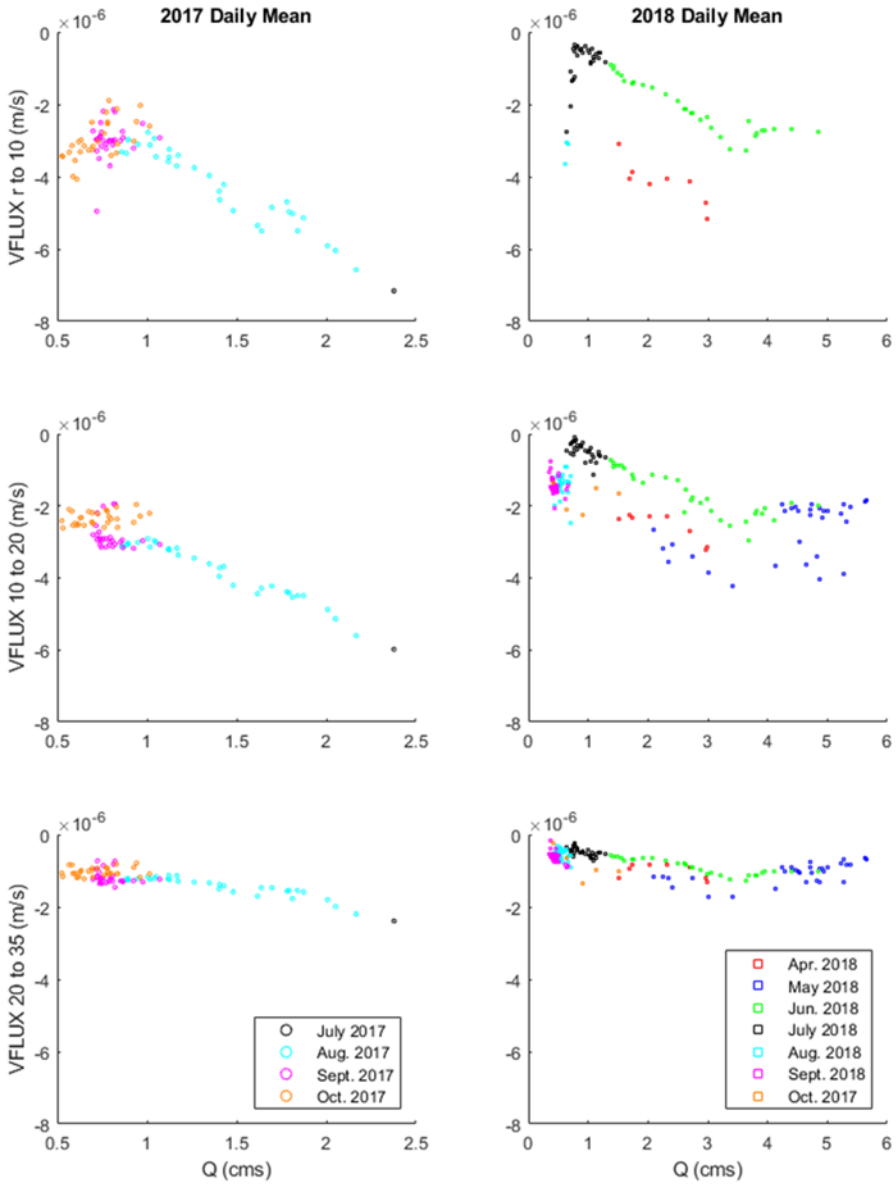

Figure 4: Relationships between estimated vertical fluxes and river discharge for A) river to 10 cm depth in 2017, B) 10-20 cm depth in 2017, C) 20-35 cm depth in 2017, D) river to 10 cm depth in 2018, E) 10-20 cm depth in 2018, and F) 20-35 cm depth in 2018. Note that the y-axis is the same between years, but the x-axis differs.

Groundwater with low DO concentrations infiltrating into the hyporheic zone may be a cause of some of the DO changes, so it is important to assess the correlation between the estimated vertical flux and the DO concentrations. An elevated water table is expected to inhibit hyporheic flow (i.e., vertical flux would be low or upwelling). In August through October of 2017, the water table was higher than in 2018 (Table 4). In general, the water table was high and peaked later in 2017 but this was not captured

in Figure 4 due to the sensor deployment and therefore VFLUX modeling time not fully overlapping with the snowmelt period of both years. In 2017 the groundwater gradually decreases throughout the season as seen in Figure 5A-C. 2018 (Figure 5D-F) has a larger range of groundwater elevations than 2017 due to 2017 not including the peak of snowmelt since it was before sensor deployment. The water table elevation increases in April 2018 at the start of snowmelt then gradually decreases throughout the rest of 2018 which can be seen most clearly in the river to 10cm depth flux (Figure 5D), but is also present in the deeper flux layers (Figure 5E and F). We see higher fluxes at higher water table elevations during both years and at all depths which is the opposite of the expectation. This may be due to PLM6 being higher on the hillslope than the riverbed and therefore showing different head gradients, or that streamflow has a greater influence on vertical flux than does water table elevation.

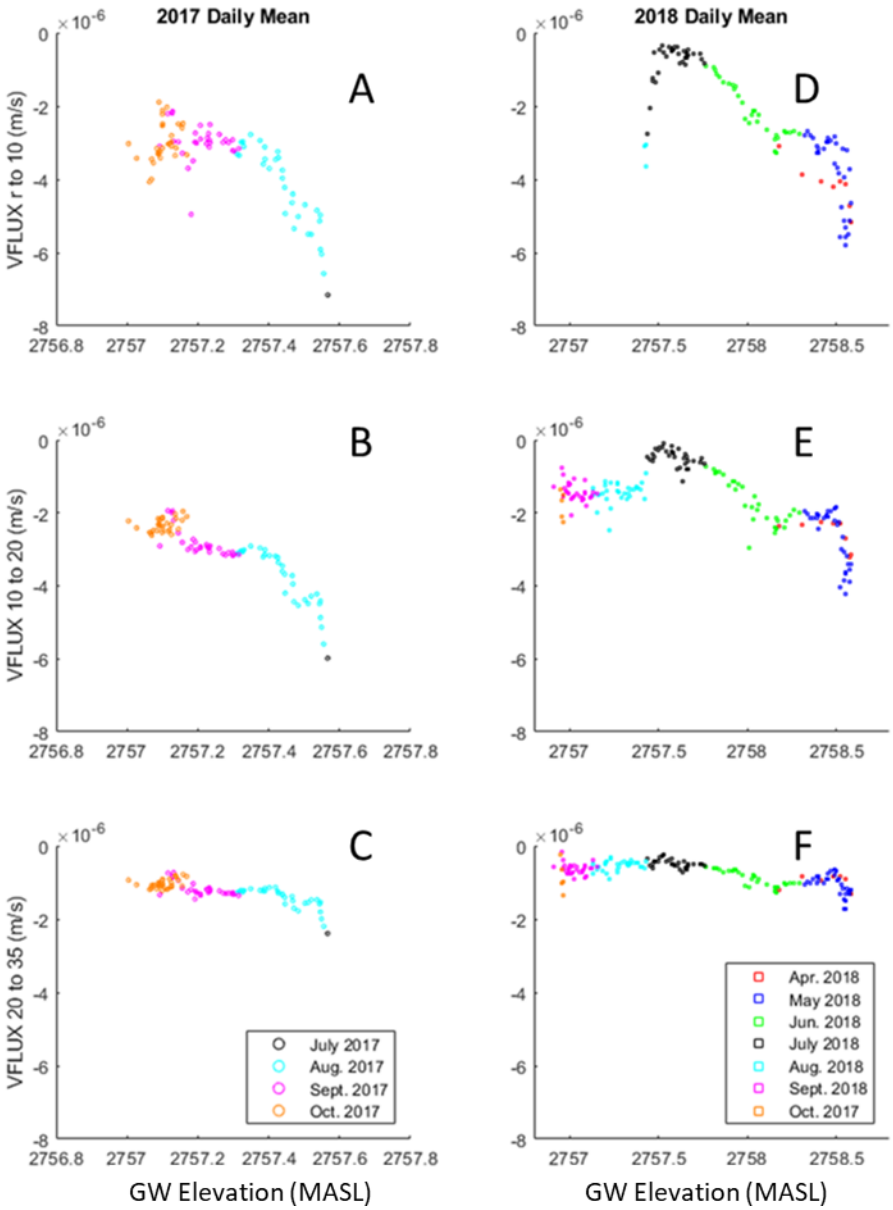

Figure 5: Relationships between estimated vertical fluxes and ground water elevation for A) river to 10 cm depth in 2017, B) 10-20 cm depth in 2017, C) 20-35 cm depth in 2017, D) river to 10 cm depth in 2018, E) 10-20 cm depth in 2018, and F) 20-35 cm depth in 2018. Note that the y-axis is the same between years, but the x-axis differs.

We plotted DO concentration against stream discharge (Figure 6) to determine if the stream was a control on DO concentrations in the streambed, especially at times of low flow which has been see in previous literature as a control. Higher discharge is expected to lead to higher vertical fluxes and therefore higher DO concentrations in the bed. While the general trends are the same as the previous Q correlation graph (Figure 4), the subsurface does exhibit some odd patterns for a few days. In Figure 6C,

we can see the DO at 20 cm depth drops in August for about 6 days, including two days of near anoxia. An irregularity also occurs in the DO records at 10 cm and 35 cm depths (Figure 6B and D), but instead of a drop to anoxia, there is a pattern of a small loop within the general decreasing linear trend of the DO concentration and stream discharge relationship. This small loop is between 1.5 to 2 cms during August with a bigger response loop at 35 cm than 10 cm. These periods of irregularity are likely due to high rainfall days that occur on August 8, 14 and 25 in 2017.

The dynamics of DO at 10 cm and 20cm compared to stream discharge (Figure 6F and 5G) show how the subsurface quickly goes anoxic in June 2018 and then stays anoxic for the rest of the deployment. Though, at 10 cm there are two times when DO concentrations rise back above anoxia for a short period of time, one in July 2018 and one in September 2018. The DO in July 2018 stays in the streambed for approximately 6 days and cannot be seen in any other layer. The DO in September 2018 stays for 14 days and one day of October 2018 at 10cm (Figure 6F) then there is a small increase at 20 cm for 2 days (Figure 6G). These DO concentration increases are will be further explored later in this thesis. The same patterns are seen in the DO saturation data (Figure 7), though the river signal is dampened and shows a slight decrease in DO saturation over time in 2017 as the temperature drops where the DO concentration shows a slight increase over time. The DO and Q relationship also shows a hysteresis loop pattern in 2018 and a linear pattern in 2017, though the 2017 pattern may be a hysteresis loop if an earlier time was recorded. The assumption that higher discharge led to higher DO concentrations in the bed holds for both years after peak snowmelt discharge.

A few linear trends are seen within the DO concentration and Q relationship and were further investigated with a correlation analysis conducted in MATLAB. A correlation showed that the Pearson correlation coefficient (R) for the August 2017 data is 0.87. 2018 had two different linear patterns one in April and May and the other in June and July. The R for each of these is -0.78 and 0.95. This means that

the DO and discharge are highly correlated in August 2017 and July 2018 when there is low flow in the river.

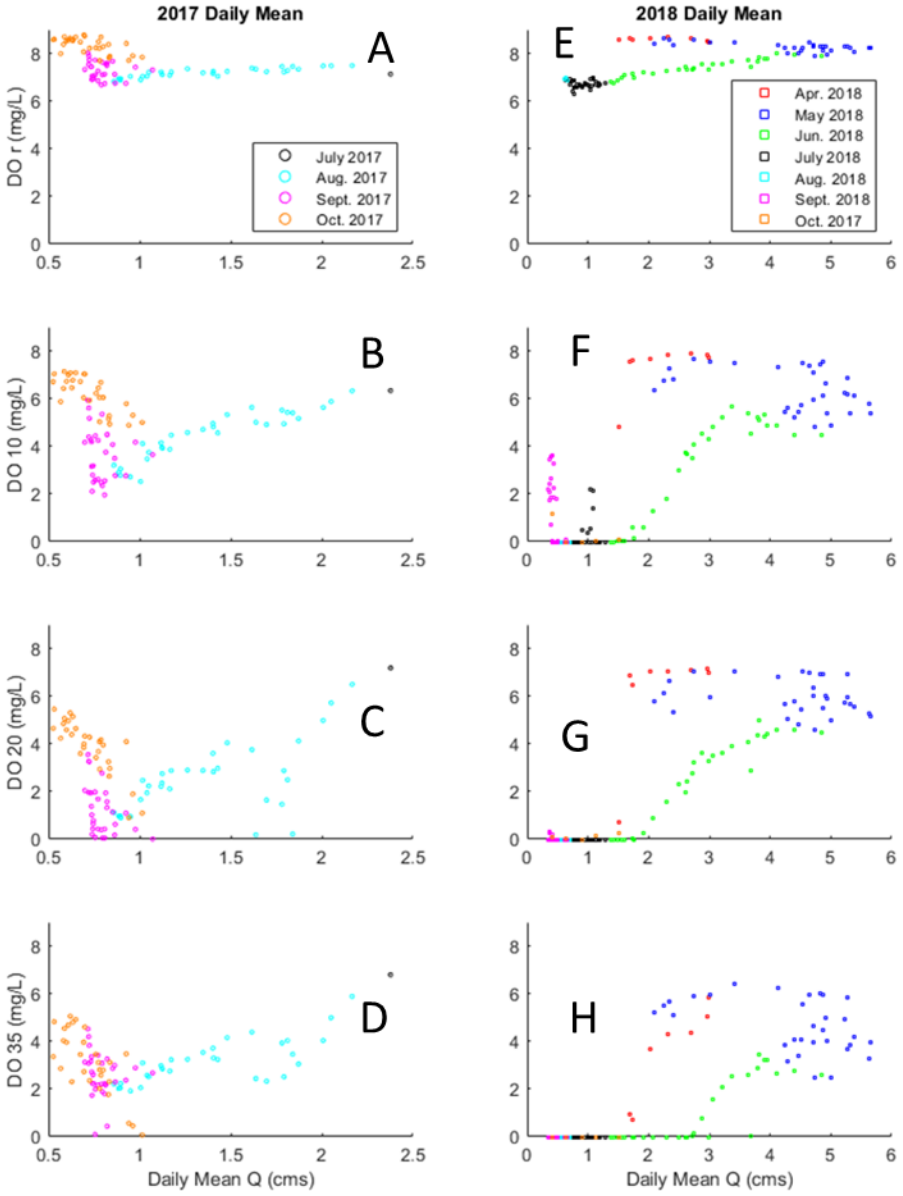

Figure 6: Relationships between estimated DO concentration and river discharge for A) river in 2017, B) 10 cm depth in 2017, C) 20 cm depth in 2017, D) 35 cm depth in 2017 E) river in 2018, F) 10 cm depth in 2018, G) 20 cm depth in 2018, and H) 35 cm depth in 2018. Note the y-axis is the same between the two years but the x-axis is different.

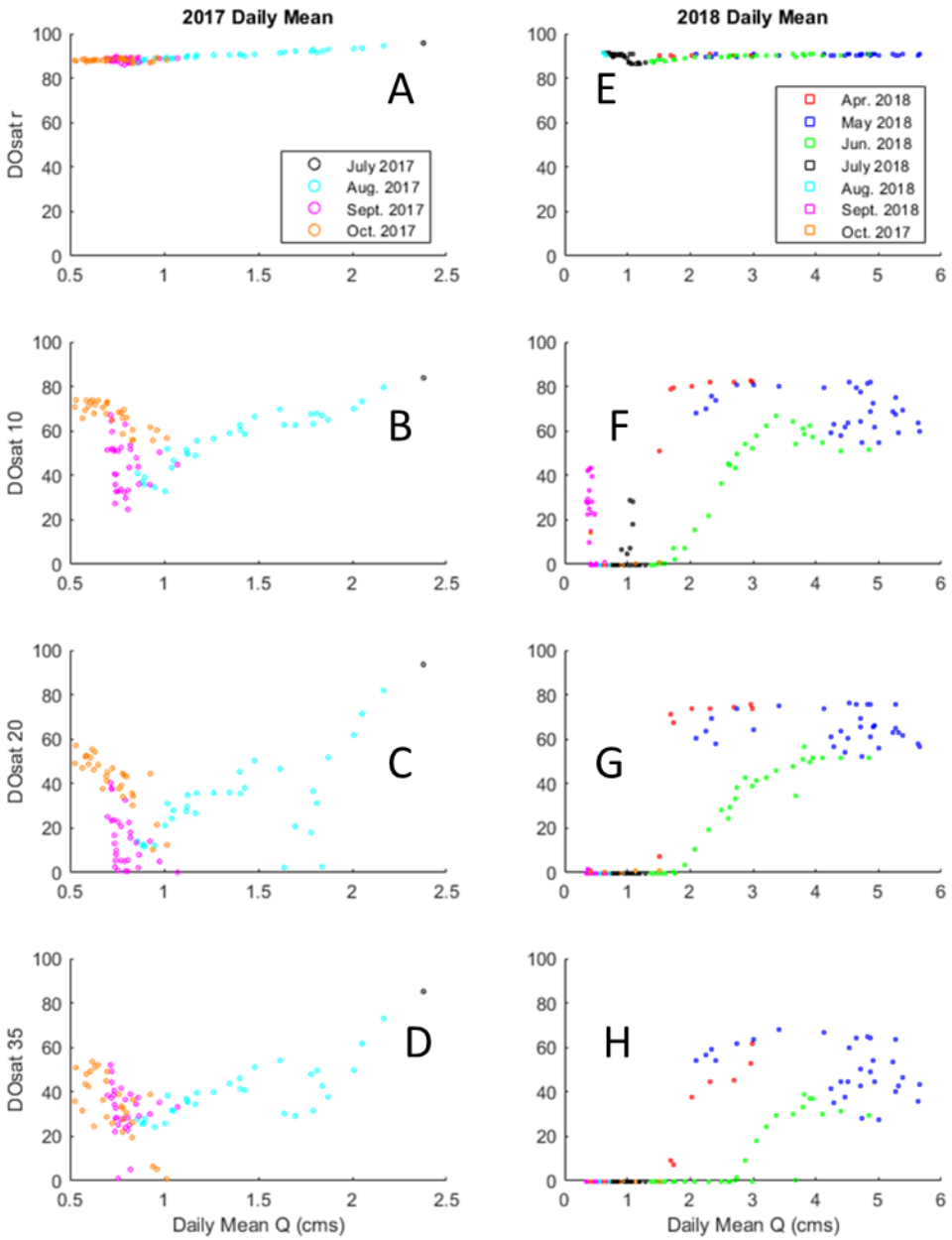

Figure 7: Relationships between estimated DO saturation and river discharge for A) river in 2017, B) 10 cm depth in 2017, C) 20 cm depth in 2017, D) 35 cm depth in 2017 E) river in 2018, F) 10 cm depth in 2018, G) 20 cm depth in 2018, and H) 35 cm depth in 2018. Note the y-axis is the same between the two years but the x-axis is different.

Generally, increased DO in subsurface is expected with increased VFLUX moving more river water into bed. This increased vertical flux also reduces the residence time of water in the hyporheic zone where microbes can consume the DO. DO concentration decreases as the magnitude of VFLUX decreases (Figure 8A-C) but October 2017 shows a steady VFLUX estimate with increasing DO

concentrations. 2018 shows a DO spike with flux in July (Figure 8D) though this pattern does not continue through deeper layers due to the bed anoxia during this time (Figure 8E and F). Figure 8C and 8F both show narrow ranges of VFLUX estimates at 20 to 35 cm depth with Figure 8F in 2018 showing the narrowest VFLUX estimates but having a wide DO range of above 6 mg/L to anoxic. The DO saturation shows similar relationships with vertical flux (Figure 9) where there is generally decreasing DO concentration with decreasing flux except for October 2017 (Figure 9A-C).

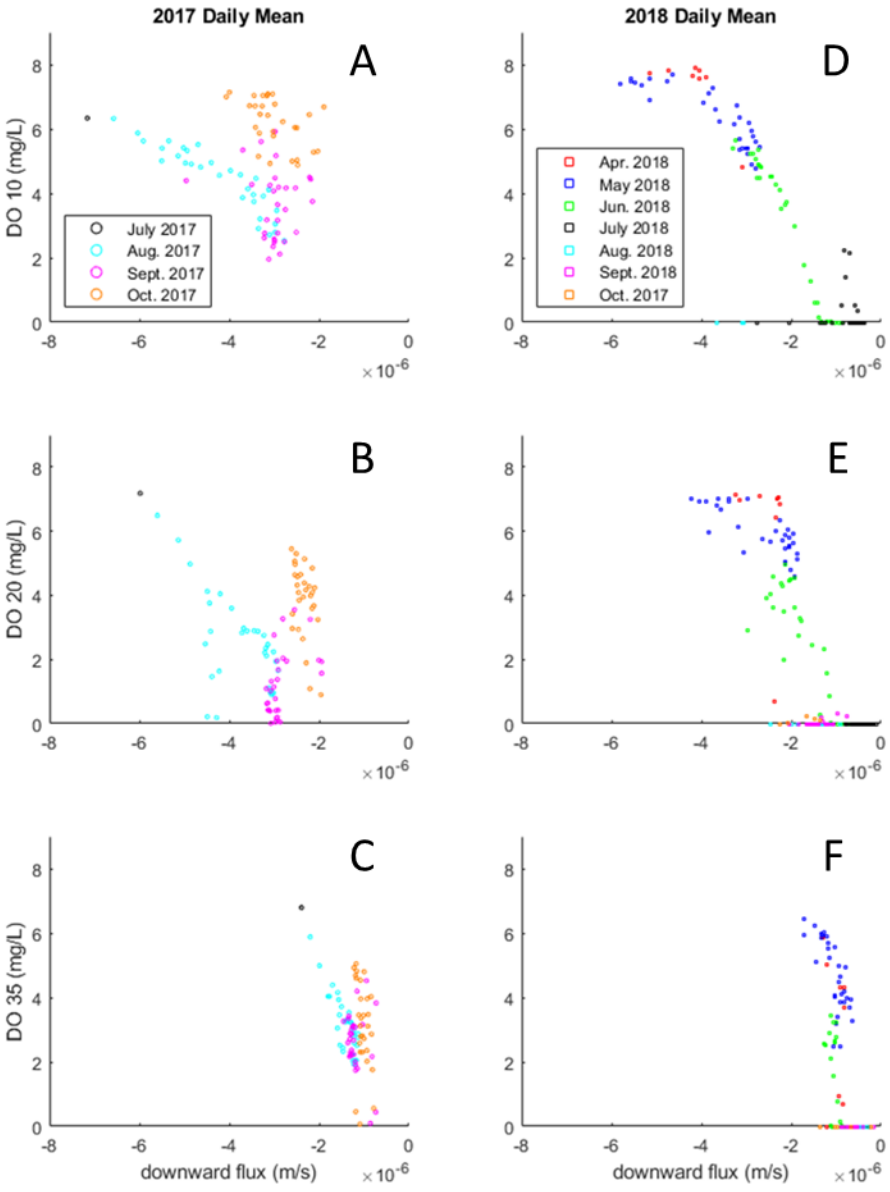

Figure 8: VFLUX versus the 'receiving' DO sensor of that flux in 2017 with A) DO concentration at 10 cm depth compared to river to 10cm VFLUX2 estimate B) DO concentration at 20cm depth compared to 10

cm to 20cm VFLUX2 estimate C) DO concentration at 35 cm depth compared to 20cm to 35cm VFLUX2 estimate and 2018 with D) DO concentration at 10 cm depth compared to river to 10cm VFLUX2 estimate E) DO concentration at 20cm depth compared to 10 cm to 20cm VFLUX2 estimate F) DO concentration at 35 cm depth compared to 20cm to 35cm VFLUX2 estimate.

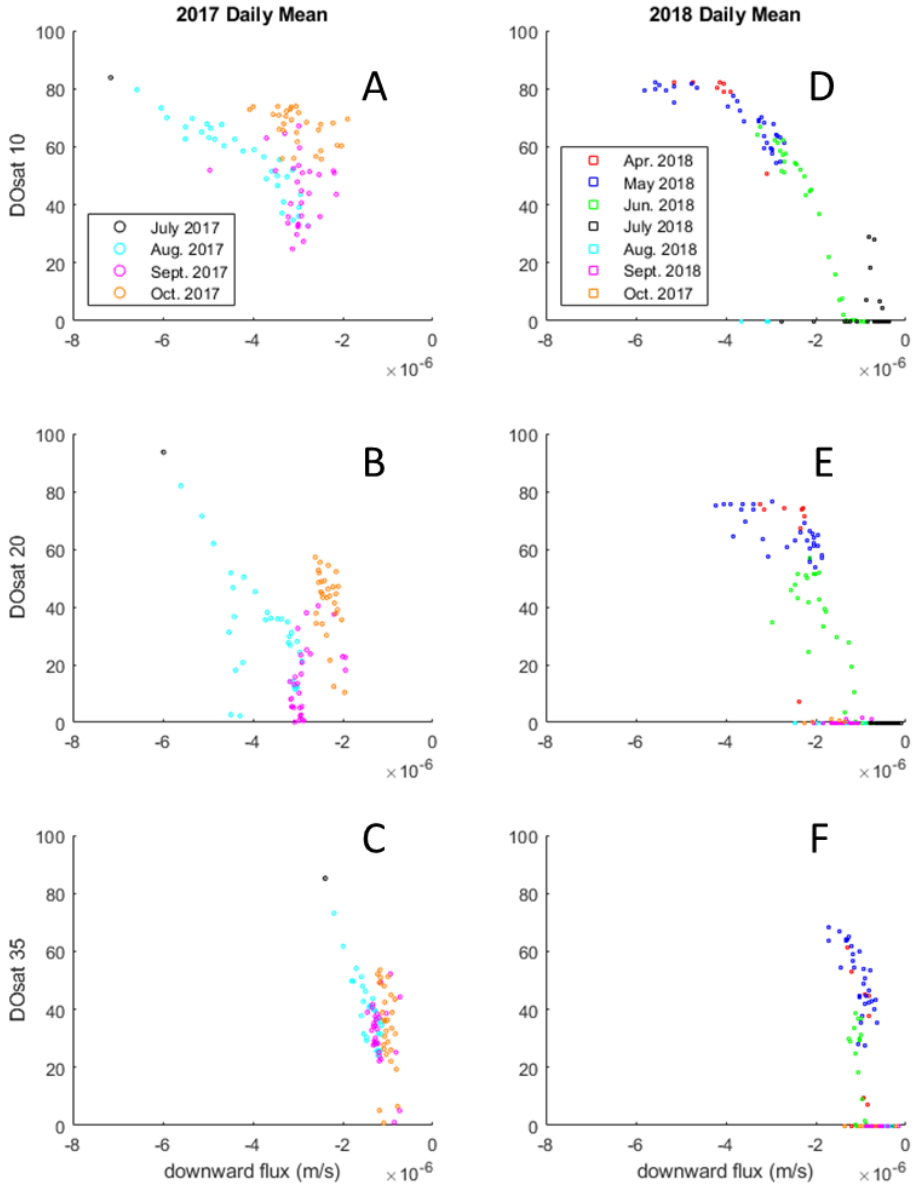

Figure 9: VFLUX versus the 'receiving' DO sensor of that flux in 2017 with A) DO saturation at 10 cm depth compared to river to 10cm VFLUX2 estimate B) DO saturation at 20cm depth compared to 10 cm to 20cm VFLUX2 estimate C) DO saturation at 35 cm depth compared to 20cm to 35cm VFLUX2 estimate and 2018 with D) DO saturation at 10 cm depth compared to river to 10cm VFLUX2 estimate E) DO saturation at 20cm depth compared to 10 cm to 20cm VFLUX2 estimate F) DO saturation at 35 cm depth compared to 20cm to 35cm VFLUX2 estimate.

ΔDO calculations over the deployment period show vastly different amplitudes and timing of removal between 2017 and 2018 (Figure 10A and C). Positive ΔDO values indicate an increase in DO

concentration between a pair of sensors (e.g. 20 cm to 35 cm), while negative values indicate a removal of DO between a pair of sensors (e.g. river to 10cm). Removal is the expected outcome due to microbial activity in the subsurface though decreasing temperatures could influence the amount of oxygen in the water along with any effects from non-linear flow paths. Times with 0 mg/L ΔDO occur from July through October 2018 (Figure 10C) due to the extended anoxic period throughout the riverbed. No other ranges are shown during this time because there was no oxygen in the incoming or outgoing water therefore the ΔDO was not calculated. The proportional change shows an extended period of -1 is during this period of anoxia (Figure 10D). This is an artifact of the calculation since there is 0 mg/L at the sensor above and below therefore there is 100% removal or -1 proportion. Positive proportions up to 1.5 are seen in the 20 cm to 35 cm calculation and smaller positive values in the 10 cm to 20 cm calculation in 2017 (Figure 10B), this is likely due to the 20cm sensors being on a different flow path than the 10 cm or 35 cm sensors.

In 2017, there is a positive ΔDO due to the 35cm sensor having more DO than the 20cm sensor for most of the year outside of a short period in early August (Figure 10A). This leads to large DO change proportions in 2017 (Figure 10B) since oxygen increased in the system with depth. An extended period of 0 occurs in 2018 ΔDO, from July through October 2018, due to the extended anoxic period. The extended period of -1 proportion in 2018 (Figure 10D) is an artifact of the calculation since there is 0 mg/L at the sensor above and below therefore there is 100% removal or -1 proportion.

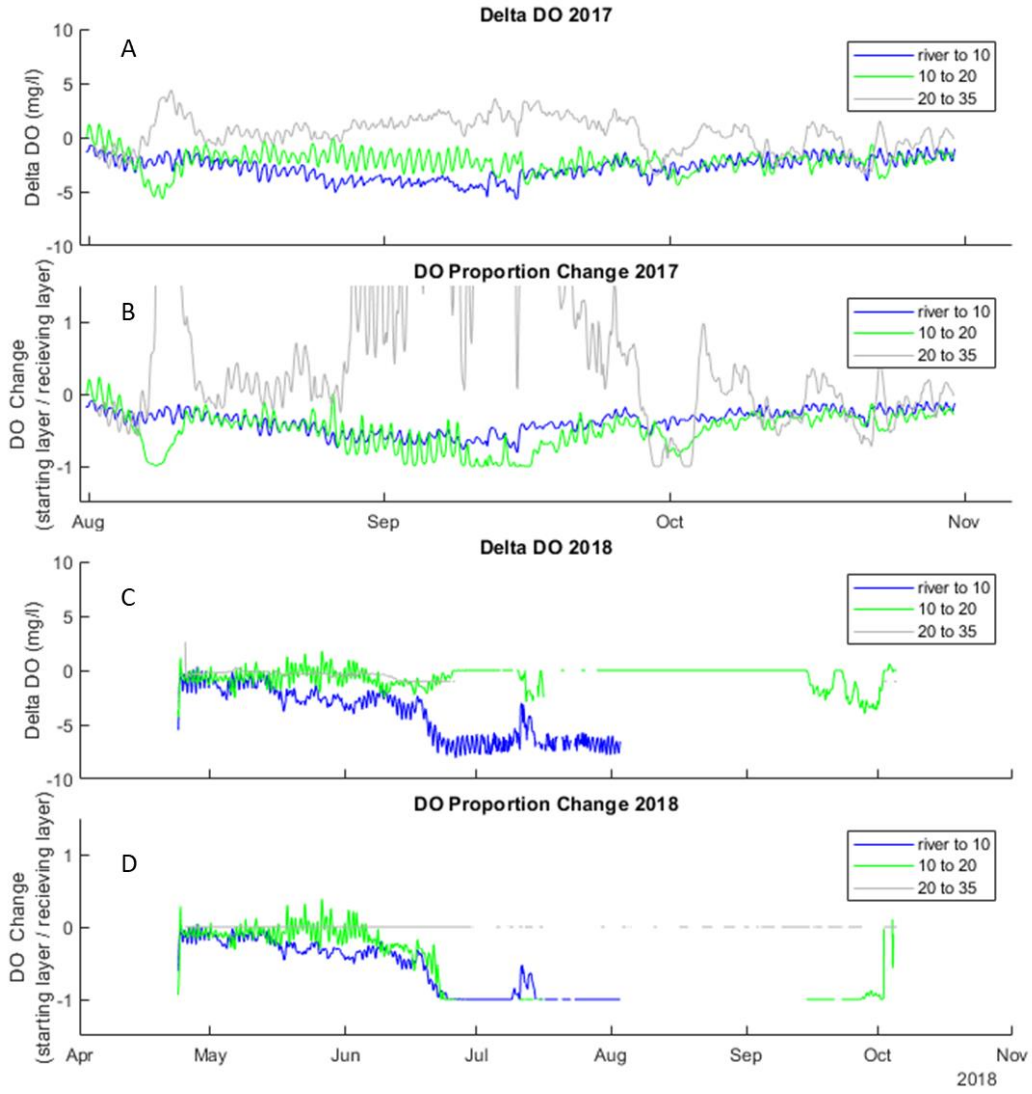

Figure 10: ΔDO for DO proportion calculations are shown grouped by year A) 2017 ΔDO B) 2017 DO proportional change C) 2018 ΔDO D) 2018 DO proportional change.

It is expected that increased discharge will increase flux and decrease DO removal. The ΔDO has a linear relationship to the stream discharge in for 2017 in the river to 10cm and 10cm to 20cm sections (Figure 11A and B) though the 20 to 35 cm shows more of a splattering of point grouped by month with July in the center of the data cluster (Figure 11C). These are very different than the patterns seen in 2018. The river to 10cm layer has a complete clockwise hysteresis loop (Figure 11D) with values for both ΔDO and Q being lower in July and August in 2018 than 2017. The deeper layers (Figure 11E and F) are mostly linear due to the extended anoxic period in the bed. Though there were a few exceptions where

removal happened. There are small amounts, up to 2 mg/L, of removal occurring in June at 10 to 20 cm (Figure 11E) along with larger spikes of removal in July and September.

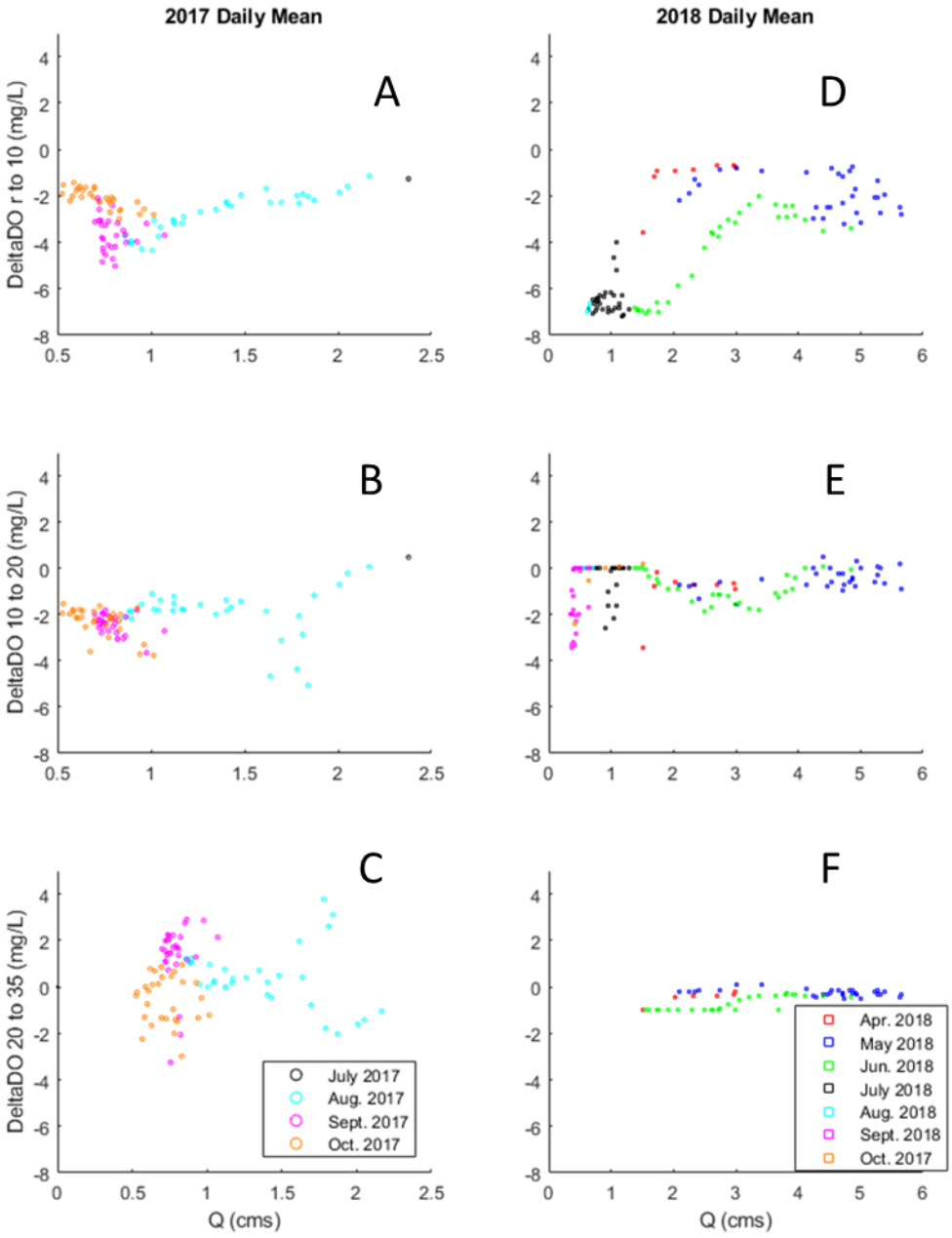

Figure 11: Relationships between estimated ΔDO and river discharge for A) river to 10cm depth in 2017, B) 10 to 20 cm depth in 2017, C) 20 to 35 cm depth in 2017, D) river to 10cm depth in 2018, E) 10 to 20 cm depth in 2018, and F) 20 to 35 cm depth in 2018. Note the y-axis is the same between the two years but the x-axis is different.

The infiltration of groundwater, which is low in DO, into the hyporheic zone may be a cause of some of the DO changes, so it is important to look at the correlation between the change in DO

concentrations and the water table elevation to determine if there are any patterns. The ΔDO and groundwater elevation seems to have a parabolic relationship in 2017 in the river to 10cm layer and in the 20 to 35cm layer (Figure 12A and C), but this pattern does not appear in the 10 to 20cm layer (Figure 12B) which shows a linear trend. Interestingly, the parabola seems to be inversed and moved to a slightly higher concentration at depth in 20 to 35 cm depth (Figure 12C) compared to river to 10cm depth (Figure 12A). This is another indication that the 20 cm sensor may be on a different flow path, but this cannot be evaluated for 2018 due to the anoxic conditions. The 2018 data show interesting dynamics at the surface interface (Figure 12D) and the previously mentioned linear pattern at depth (Figure 12E and F) with deviations during rain events. In the river to 10 cm layer (Figure 12D) there is a steep increase in June DO removal compared to GW, which is otherwise steady except for the few increasing water table elevation days in April which appear as a nearly horizontal line.

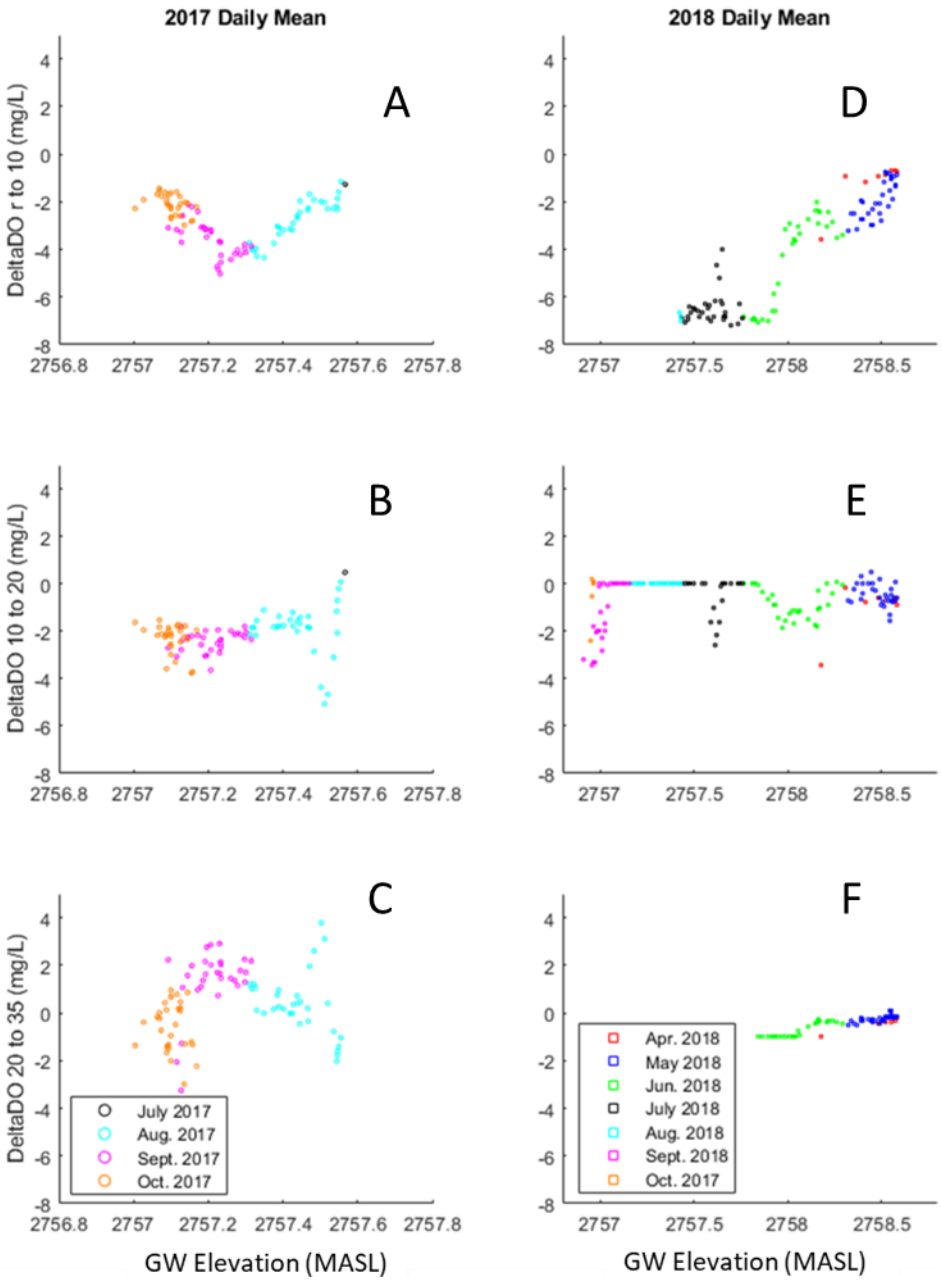

Figure 12: Relationships between estimated ΔDO and groundwater elevation for A) river to 10cm depth in 2017, B) 10 to 20 cm depth in 2017, C) 20 to 35 cm depth in 2017, D) river to 10cm depth in 2018, E) 10 to 20 cm depth in 2018, and F) 20 to 35 cm depth in 2018. Note the y-axis is the same between the two years but the x-axis is different.

The relationship between the ΔDO and streambed temperature was investigated to look at relationships between increased temperature which is expected to lead to increased microbial activity and DO removal. This trend of increased temperature leading to increased removal is evident when looking at the 10 cm depth temperature compared to the river to 10 cm depth ΔDO. DO removal

steadily decreases over September and October as the temperature falls (Figure 13A). This pattern dampens in as the depth increases leading to a nearly horizontal line at 20 cm depth and higher temperatures leading to higher DO addition at 35 cm. (Figure 13 B and C). DO removal happens in a similar pattern in the river to 10cm layer during 2018, where increased temperatures lead to increased removal (Figure 13D). Due to the extended anoxic period in the subsurface, not much can be said for the removal patterns and their relationship to temperature in the 2018 deep subsurface (Figure 13E and F).

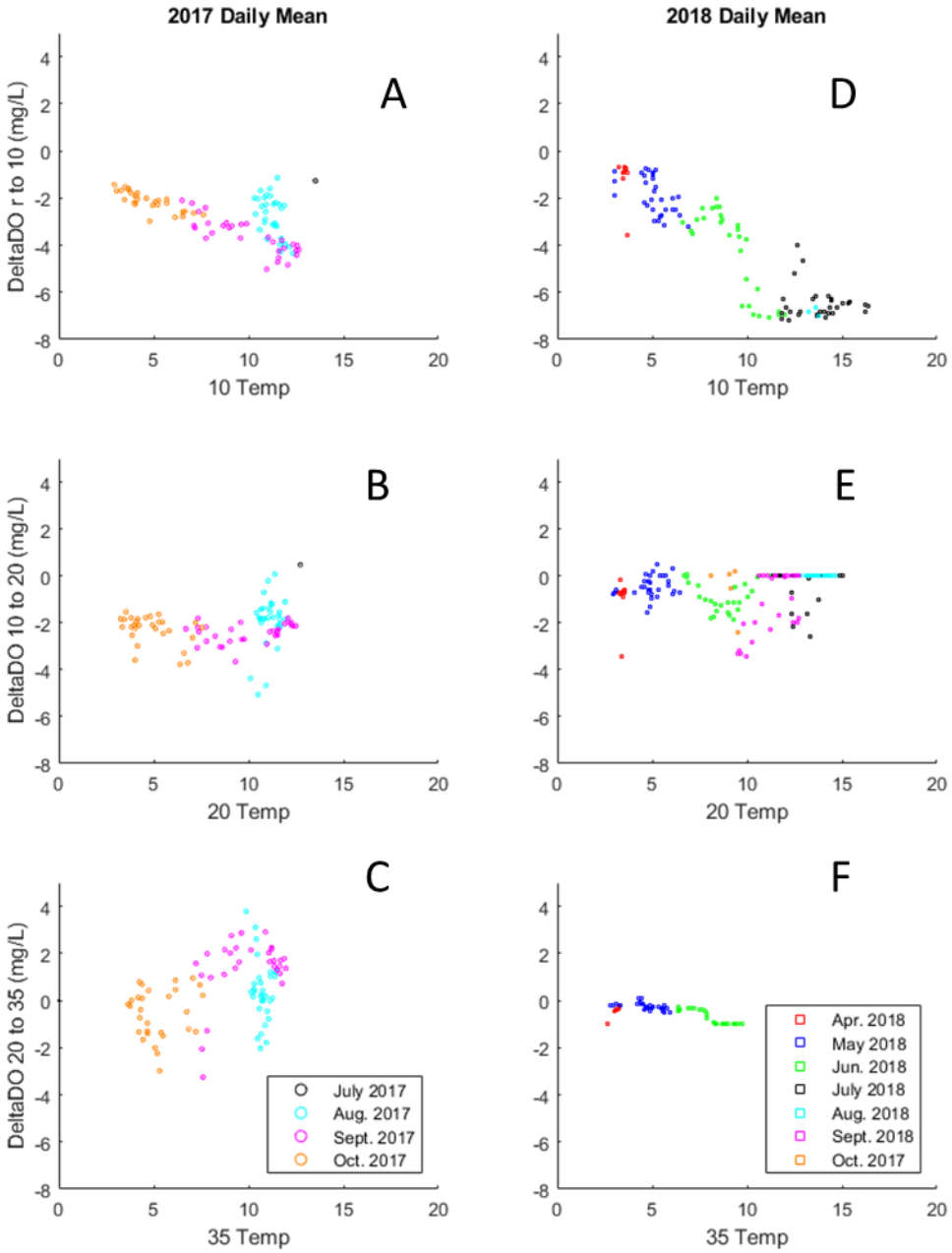

Figure 13: Relationships between estimated ΔDO and temperature for A) river to 10cm depth in 2017, B) 10 to 20 cm depth in 2017, C) 20 to 35 cm depth in 2017, D) river to 10cm depth in 2018, E) 10 to 20 cm depth in 2018, and F) 20 to 35 cm depth in 2018.

Time Periods of Interest:

We observe a few strong changes in vertical flux estimates throughout the 14-month record. On September 23, 2017, the VFLUX estimate from river to 10 cm depth almost doubles in magnitude, while there is a muted change in 10 cm to 20 cm depth and 20 cm to 35 cm depth (Figure 14E). This big change in magnitude does not coincide with a large storm (Figure 14A) or a change in discharge (Figure

14B), rather, it occurs with a substantial cooling of the air and river temperatures (Figure 14A and C) during a period of a few days of low level precipitation. There is a 24-hour period missing from the 2017 stream discharge record from September 30 at noon to October 1 at noon. From observing surrounding data, the discharge likely linearly increases during this time. Given the reliance of VFLUX on temperatures, this strong change is not a surprising result. It was not a result previously observed in the literature so it serves as a point of caution as it is unclear if the flux changed this much in such a short time period.

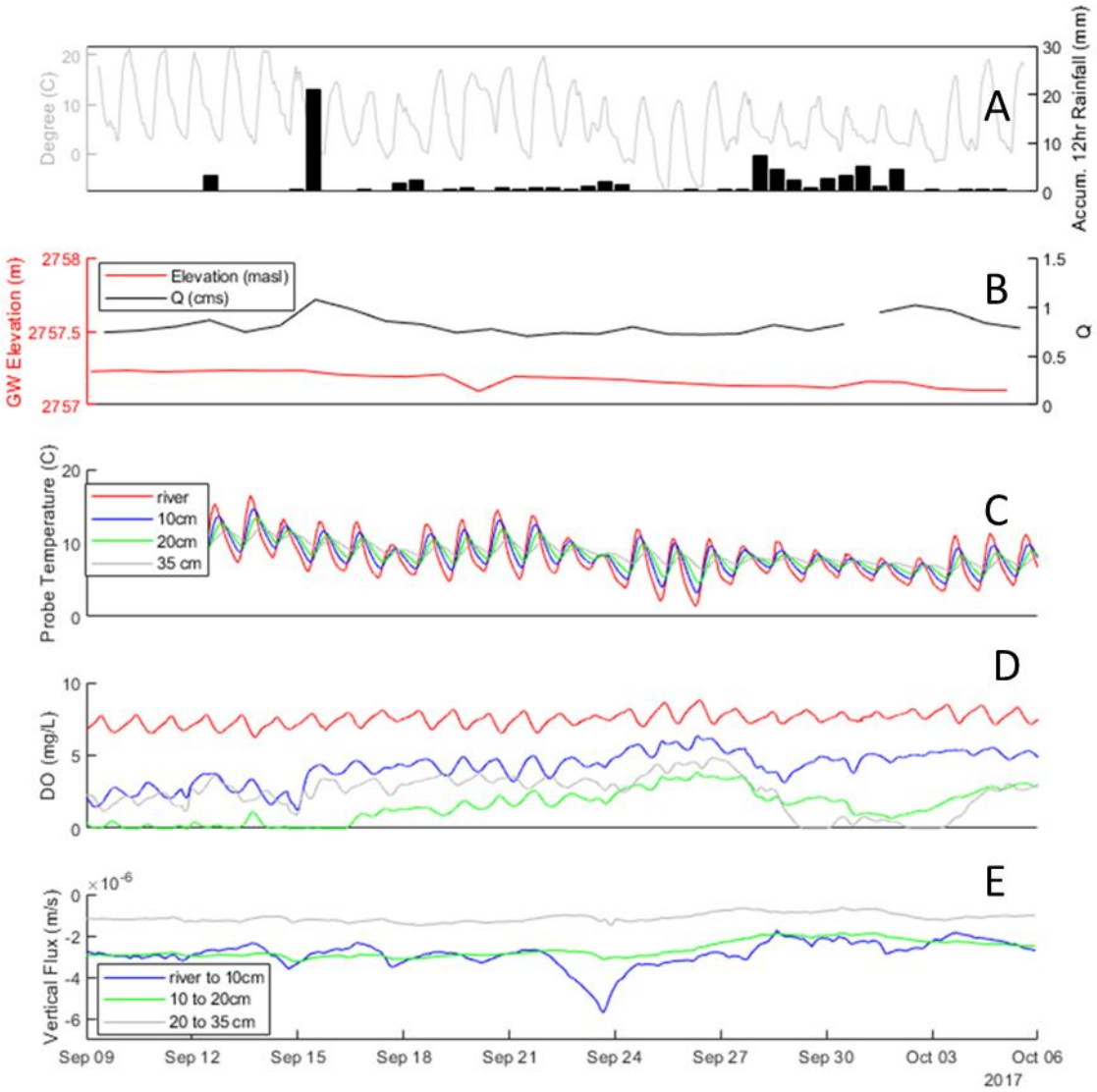

Figure 14: Event of interest, September 9 to October 5, 2017 timeseries of A) air temperature and 12-hr

accumulated rainfall, B) groundwater and stream discharge, C) sensor temperature, D) dissolved oxygen concentrations, and E) VFLUX estimates.

Another period of interest is June 9 to June 26, 2018. On June 18, 2018, a substantial storm (Figure 15A) causes a spike in the hydrograph (Figure 15B) and dampening of the diurnal temperature signal (Figure 15C) causing a small increase in magnitude of all three vertical flux estimates (Figure 15E). This also causes a flattening of the DO concentration signal at the river, 10 cm, and 20 cm depth, though no effect is seen at 35 cm depth due to its anoxia (Figure 15D). The change in the estimated vertical flux is consistent with the overall pattern of increased vertical fluxes at times of higher streamflow, and the magnitude of change both in the streamflow and the vertical flux estimates do not exceed those observed earlier in the snowmelt period. Thus, these appear to be reasonable vertical flux responses to streamflow.

There is also a gradual decrease in DO concentration to anoxia during this period from June 9 to June 26, 2018. (Figure 15D). While initially we presumed this was due to the storm event on June 18th, this does not seem to be correct as the 35 cm depth goes anoxic on June 13th before the storm begins. This anoxic period is likely caused by the decreased stream discharge and high temperatures.

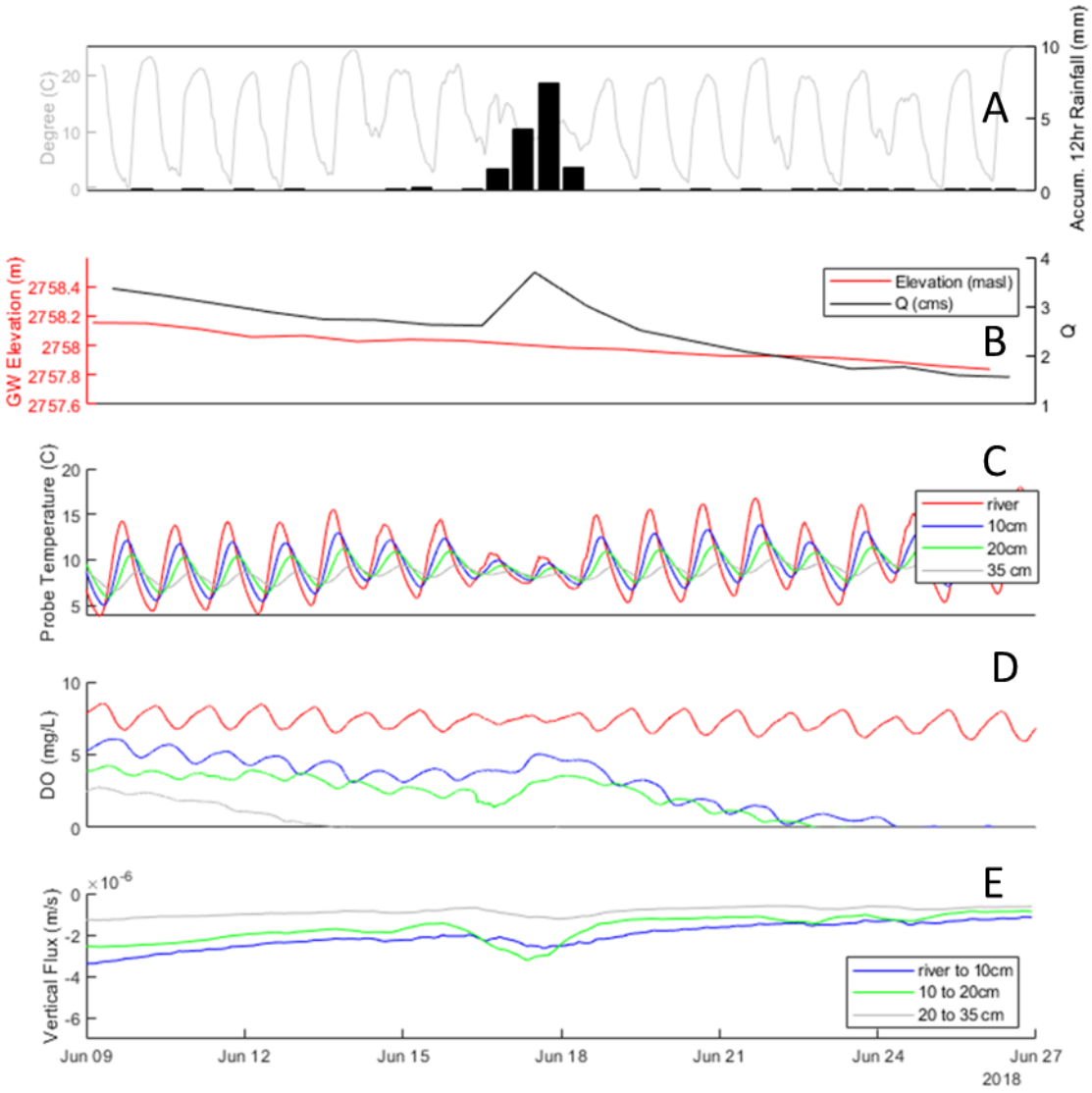

Figure 15: Event of interest, June 9 to June 26, 2018 timeseries of A) air temperature and 12-hr accumulated rainfall, B) groundwater and stream discharge, C) sensor temperature, D) dissolved oxygen concentrations, and E) VFLUX estimates

Another period of interest with odd DO patterns is September 11 – September 28, 2018. Though no changes are seen on September 14 in precipitation (Figure 16A) or discharge (Figure 16B), a pulse of DO occurs at 10 cm depth (Figure 16D). This pulse of DO disappears after the storm event on September 19th and 20th. This storm causes increased discharge (Figure 16B) and dampened temperature patterns. The river to 10cm flux was already removed (Figure 16E) because the 10 cm depth peak daily temperature is higher than the river temperature peak daily temperature which violates model assumptions (Figure 16C). The reason for DO reappearing at depth could be caused by reduced

biological activity within the microbial community due to the decreasing fall temperatures and potentially having used up available nutrients. The DO concentration dipping after the storm is likely due to the storm transporting organic material along with DO into the subsurface. This increase in nutrients revitalizes the microorganisms causing a temporary increase in DO removal.

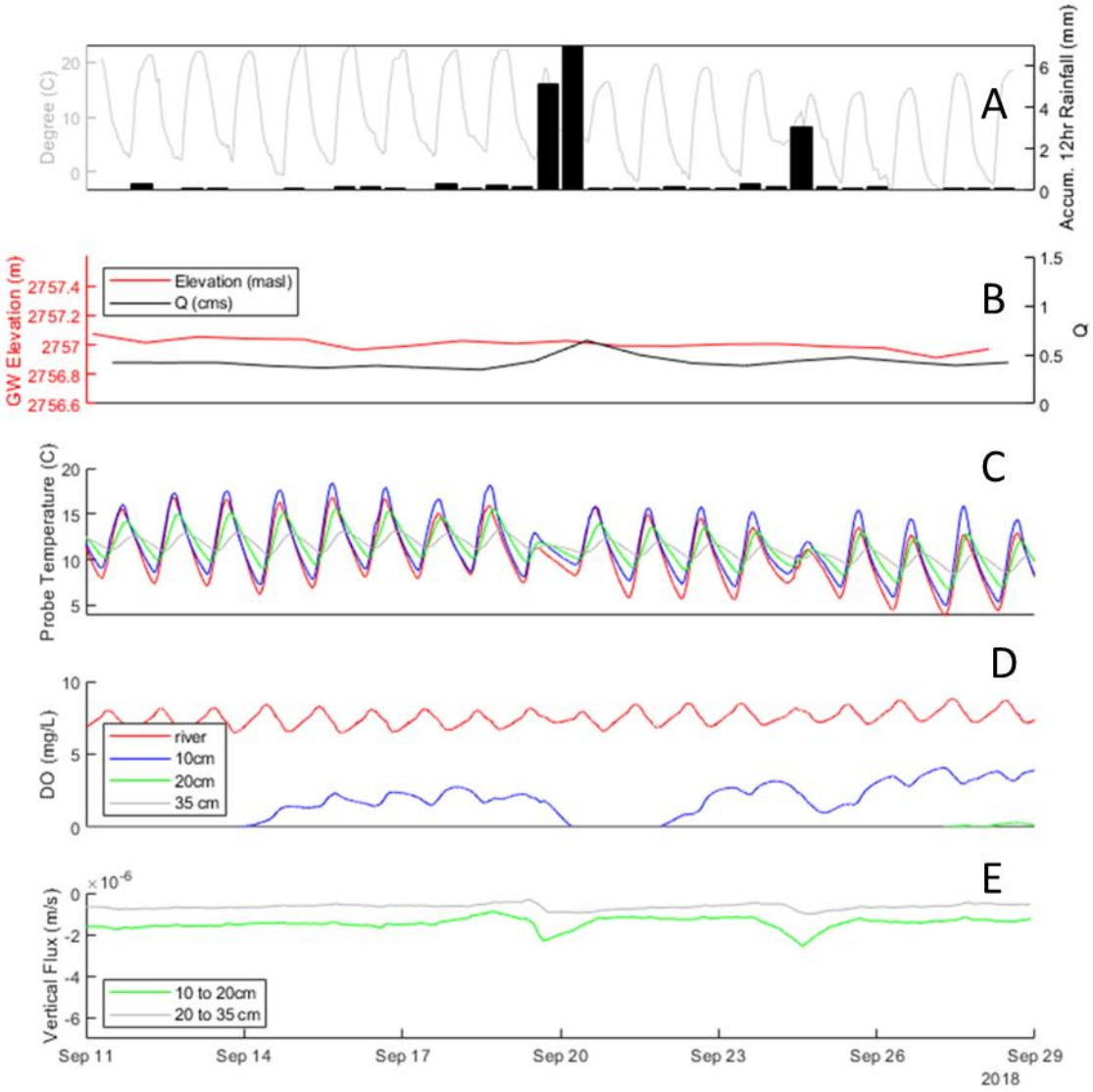

Figure 16: Event of interest, September 11 – September 28, 2018 timeseries of A) air temperature and 12-hr accumulated rainfall, B) groundwater and stream discharge, C) sensor temperature, D) dissolved oxygen, and E) VFLUX estimates

Discussion:

Model Reliability:

Model uncertainty was evaluated with a Monte Carlo analysis and a sensitivity analysis, both of which are built in as functions of the VFLUX2 model. Confidence intervals were evaluated with a Monte Carlo analysis of 1000 realizations using varying thermal parameters all falling within two standard deviation of the value we selected, both the value and the deviation were the same as defined by Bryant et al. (2020) for the East River Streambed. Substantial deviations or widening of these confidence intervals for the simulations would indicate that we had substantial uncertainty in the output. The Monte Carlo analysis for 2017 and 2018 (Figure 17) indicates that there are no abrupt changes at any time and that changes are small relative to the magnitude of the confidence.

However, during rapid changes in the predicted flux, the confidence intervals narrow substantially, which is counterintuitive. Lautz (2012) has shown that during these times directly after a rapid change the fluxes generally do not fall within the 95% confidence interval due to smoothing of the modeled fluxes relative to lab measured fluxes. This pattern of narrowed confidence intervals during rapid change is seen in the late September 2017 river to 10 cm flux decrease and in the late April- early May flux increase. The flux estimates for mid-August through early October in 2017 are nearly the same and have overlapping confidence intervals in the Monte Carlo analysis (Figure 17) except for the large storm in late September. In 2018 there are overlapping flux estimates for all fluxes for mid-June to late July.

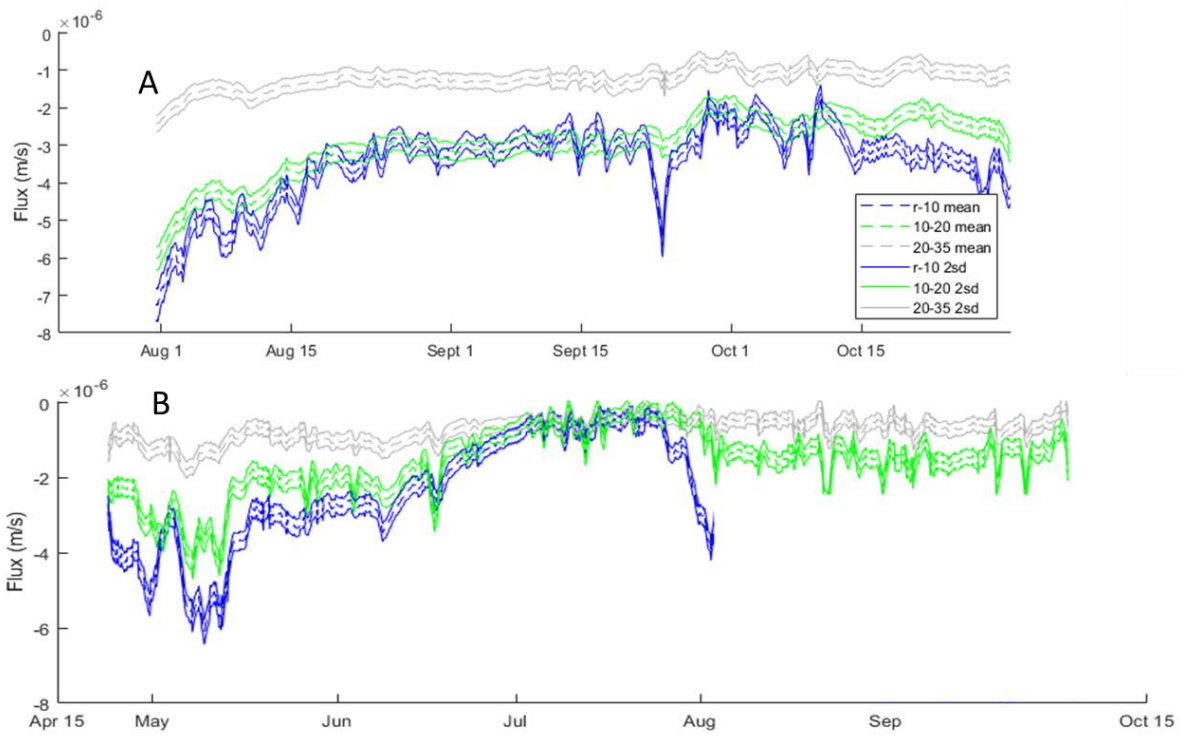

Figure 17: Monte Carlo analysis for 2017 and 2018 with the mean and 95% CI shown.

A sensitivity analysis was conducted for plus or minus two standard deviations and median values of the thermal parameters (Appendix Figure A1-A6). The sensitivity analysis showed that model is more sensitive to changes in porosity than other factors like thermal dispersivity or sediment heat capacity. However, this sensitivity is likely due to the larger standard deviation of the porosity compared to other model parameters. VFLUX has previously been shown to be most sensitive to changes in thermal conductivity of the sediment-water matrix and volumetric heat capacity of the sediment (Latuz, 2013). Our thermal conductivity range is very narrow. This narrowness leads to more certainty in our values. Our volumetric heat capacity does show some variability, which increases with depth, but due to our high confidence these values do not vary enough to be considered problematic.

System Dynamics:

The hydrologic regime changes greatly over the two years and seems to account for some of the changes in streambed DO. The DO dynamic is particularly interesting when comparing the pattern of

anoxia in the two years. There is an extended anoxic period in the subsurface throughout the summer and fall of 2018, but in 2017 there were only short periods of anoxia at 20 and 35cm depth. 2017 had anoxia mainly at the 20cm sensor with no anoxia above or below. The DO went anoxic linearly with depth in 2018 starting at 35 cm depth and working its way to the 10 cm depth. In 2018 the streambed was anoxic at all depths from late June until the sensors were removed in early October, with a few incursions of DO at 10 cm and 20 cm depth. Our findings of downwelling during snowmelt and high flow agrees with previous studies (Soulsby et al., 2001), although no upwelling was seen even at the lowest flows. Because winter was not modeled due to the lack of diurnal temperature signal (and ice buildup in the channel), it is possible that upwelling was happening in the winter baseflow period when head differential may be smaller between the stream and groundwater (Malcolm et al. 2004).

Some of the 2017 and 2018 DO to Q correlations show that in 2017 there are higher DO values at corresponding Q's than in 2018. This finding indicates that even when the flow is at the same level there is less oxygen in the water at all depths in the streambed. Higher stream flow should lead to high vertical fluxes which should lead to high streambed DO. Therefore, having increased DO in 2017 at the same discharge rate points to increased microbial activity causing the difference in DO in the subsurface in 2018.

The DO saturation condition is nearly constant in the river for 2017 and May through October of 2018 (Figure 3E and Table 7). However, a large dip in subsurface DO saturation happens in August 2017 (Figure 3E). This is likely due to an increase in streambed microbial activity as the summer temperatures increase occurs which would likely ramp up biological activity. This is seen to happen again on a larger scale in the streambed in June 2018 which likely happened due to the combined factors of increased temperature and extreme low flows (Figure 3E).

In 2017 the DO dynamics are non-linear. For most of the season the 35 cm depth has higher DO than 20 cm especially in September where the 35cm DO was nearly the same as the 10cm DO, while 20 cm was hypoxic or anoxic. All of this points to the 20cm sensor being on a different flow path from the other sensors. This situation violates one of the model assumptions for VFLUX though this estimate can still be used as an order of magnitude measurement or within 20% of the flux if the vertical flux is larger than the lateral flux (Lautz 2010). There could be on a different flow path due to heterogenous sediment (Malenda et al., 2019) meaning that a large cobble slightly upstream of the probe could be diverting the flow at this depth by being a physical barrier.

At low flow and baseflow conditions, DO in the subsurface is heavily influenced by storm events and controlled by the flux of water into the subsurface (Figure 8). This situation is seen in July and September when the DO increases from anoxia to 2 mg/L, then nearly 4 mg/L (Figure 6). During snowmelt and the hydrograph recession, these storm events have a dampened effect on DO transport into the subsurface as is seen in August 2017 (Figure 6) compared to low flow. Small stream velocity changes can have large and delayed changes on the DO dynamics of streams (Kaufman et al. 2017).

From focusing on irregularities in the vertical flux estimates and DO dynamics we can learn about how the hyporheic zone behaves in response to different influences. During September 9 to October 5, 2017 we see that increased temperature gradients due to cold fronts can lead to changes in the flux estimates (Figure 14) because of the temperature sinusoid processing that VFLUX2 is based on though these may be showing real changes in the vertical flux. The events during June 9 to June 26, 2018 and September 11 – September 28, 2018 show that at low flows both increased discharge, typically due to storm events, and changes in microbial activity due to temperature can have noticeable effects on the concentration and spatial variability of DO (Figure 15 and 16).

As expected, the ΔDO varied between the two years. In addition, ΔDO also varied seasonally within the year. In 2017 the proportion of DO removed over 10 cm increased continually throughout the season until the beginning of September when the rates began to decrease as temperatures began to fall, so we would expect that the streambed microbial communities were less active. In 2018 there was an increased amount of removal and a continuous increase in the removal rate during the whole season, until the subsurface went completely anoxic. ΔDO also peaked during storm events (Figure 3A and B, Figure 10A and C) which has also been noted in other studies (O'Connor et al. 2012).

Our understanding of the ΔDO is limited by the modeling and assumptions underpinning the VFLUX2 model. Because the ΔDO calculations are based on vertical flux estimates, any error in these carries over into the ΔDO calculations. There is also the added assumption that all flow is purely vertical as the distance used with the velocity estimate to find the travel time was the vertical component of sensor spacing. Though, it is unlikely that the flow path is truly vertical especially at the 20cm sensor. Violation of this assumption could add to the errors in tracking a parcel of water back through time to "pair" the DO concentrations for removal estimates. The ΔDO estimates represent the average change between two locations over a period of two hours due to the timing of the VFLUX modeled velocities. Due to this, it is not exact for any point in time. The ΔDO travel time was capped at a three-day maximum as some vertical flux values were small enough that the travel time was too long to seem feasible in this system, though some studies have seen travel times in excess of three days in other heterogeneous systems (Sawyer and Cardenas, 2009).

These DO dynamics are of vital importance to fish spawning and salmonid survival (Malcolm et al. 2003). The East River DO dynamics are heterogeneous in time which has been seen in other rivers (Malcolm et al. 2003 and Malcolm et al. 2004) though the length of these studies were shorter. More long-term work needs to be done to get a full picture on how DO dynamics are effected by physical drivers under different water conditions. Studies have pointed to changes in flux in this reach mainly

being dominated by flow path direction and length than hydrologic seasonality while the stream overall has varied hyporheic dynamics typically due to sediment differences (Malenda et al., 2019). This difference in hyporheic flow due to sediment differences is also seen in other more dynamic landscapes though it was noted that seasonal differences were still important (Martone et al., 2020).

Conclusion:

Anoxia occurs in the subsurface due to change in flow conditions between the water years as small changes in stream velocity can lead to large changes in hyporheic DO dynamics (Kaufman et al. 2017). The low flow in 2018 leads to increased biotic activity until September 2018 and decreased DO in all layers of the subsurface. At times of low flow, storm events have major effects on streambed DO dynamics when head differentials between the stream and the groundwater are high, which forces oxygenated river water into the streambed as is seen in 2018 during the July and September storm events.

Another important finding is that the sensors are not all on the same flow path. The 2017 data shows that the 20cm sensor is on a different flow path with decreased DO compared to the 10cm and 35cm sensors, which has related DO concentration levels. The 20cm sensors also shows different DO response patterns to storm events in both years. All of this points to the 20cm sensor being on a different flow path than both the 10cm and 35cm sensors, which is not uncommon for this stream due to its heterogeneous sediment (Nelson et al. 2019).

This research has advanced our understanding of the dependence of DO in both the streambed and open channel on stream-groundwater exchanges through a novel approach at analyzing long term hyporheic DO data for an alluvial sub-alpine stream. More work still needs to be done to pair these physical controls with biological controls by investigating the stream metabolism at this site.

Bibliography:

Baxter CV, Hauer FR (2000) Geomorphology, hyporheic exchange, and selection of spawning habitat by bull trout (Salvelinus confluentus). Can J Fish Aquat Sci 57(7):1470–1481. https://doi.org/10.1139/f00-056

Briggs MA, Lautz LK, Buckley SF, Lane JW (2014) Practical limitations on the use of diurnal temperature signals to quantify groundwater upwelling - Journal of Hydrology https://doi.org/10.1016/j.jhydrol.2014.09.030

Bryant SR, Sawyer AH, Briggs MA, Saup CM, Nelson AR, Wilkins MJ, Christensen JN, Williams KH (2020) Seasonal manganese transport in the hyporheic zone of a snowmelt-dominated river (East River, Colorado, USA). Hydrogeology Journal (https://doi.org/10.1007/s10040-020-02146-6)

Carroll R, Williams K (2019) Discharge data collected within the East River for the Lawrence Berkeley National Laboratory Watershed Function Science Focus Area (water years 2015–2018), Watershed Function SFA. https://doi.org/10.21952/WTR/1495380

Cozzetto KD, Bencala KN, Gooseff MN, and McKnight DM (2013), The influence of stream thermal regimes and preferential flow paths on hyporheic exchange in a glacial meltwater stream, Water Resour. Res., 49, 5552–5569, doi:10.1002/wrcr.20410.

Findlay S (1995), Importance of surface-subsurface exchange in stream ecosystems: The hyporheic zone, Limnology and Oceanography, 40, doi: 10.4319/lo.1995.40.1.0159.Gordon RP, Lautz LK, Briggs MA, McKenzie JM (2012) Automated calculation of vertical pore-water flux from field temperature time series using the VFLUX method and computer program. J Hydrol 420:142–158. https://doi.org/10.1016/j.jhydrol.2011.11.053

Grimm NB, Fisher SG (1984) Exchange between interstitial and surface water: Implications for stream metabolism and nutrient cycling. Hydrobiologia 111, 219-228

Hatch CE, Fisher AT, Revenaugh JS, Constantz J, and Ruehl C (2006), Quantifying surface water–groundwater interactions using time series analysis of streambed thermal records: Method development, Water Resour. Res., 42, W10410,doi:10.1029/2005WR004787.

Hubbard SS, Williams KH, Agarwal D, Banfield J, Beller H, Bouskill N, Brodie E, Carroll R, Dafflon B, Dwivedi D, Falco N, Faybishenko B, Maxwell R, Nico P, Steefel C, Steltzer H, Tokunaga T, Tran PA, Wainwright H, and Varadharajan C (2018). The East River, Colorado, Watershed: A mountainous community testbed for improving predictive understanding of multiscale hydrological–biogeochemical dynamics. Vadose Zone J. 17:180061. doi:10.2136/vzj2018.03.0061

Ingebritsen SE, Sanford WE. (1998) Groundwater in Geologic Processes. xxi 341 pp. Cambridge, New York, Melbourne. ISBN 0 521 49608 X. *Geological Magazine, 136*(6), 697-711. doi:10.1017/S0016756899363329

Irvine DJ, Lautz LK, Briggs MA, Gordon RP, McKenzie JM (2015) Experimental evaluation of the applicability of phase, amplitude, and combined methods to determine water flux and thermal diffusivity from temperature time series using VFLUX 2. J Hydrol 531:728–737. https://doi.org/10.1016/j.jhydrol.2015.10.054

Jensen, Jannick & Engesgaard, Peter. (2011) Nonuniform Groundwater Discharge across a Streambed: Heat as a Tracer. Vadose Zone Journal. 10. 10.2136/vzj2010.0005.

Kaufman MH, Cardenas MB, Buttles J, Kessler AJ, and Cook PLM (2017), Hyporheic hot moments: Dissolved oxygen dynamics in the hyporheic zone in response to surface flow perturbations, Water Resour. Res., 53, 6642– 6662, doi:10.1002/2016WR020296.

Keery J, Binley A, Crook N, Smith J. (2007) Temporal and Spatial Variability of Groundwater-Surface Water Fluxes: Development and Application of an Analytical Method Using Temperature Time Series. Journal of Hydrology. 336. 1-16. 10.1016/j.jhydrol.2006.12.003.

Larsen, Laurel & Woelfle-Erskine, Cleo. (2018) Groundwater Is Key to Salmonid Persistence and Recruitment in Intermittent Mediterranean-Climate Streams. Water Resources Research. 54, 10.1029/2018WR023324.

Lautz LK. (2010) Impacts of nonideal field conditions on vertical water velocity estimates from streambed temperature time series, Water Resour. Res., 46, W01509, doi:10.1029/2009WR007917.

Lautz LK. (2012) Observing temporal patterns of vertical flux through streambed sediments using time-series analysis of temperature records, Journal of Hydrology, Volumes 464–465, Pages 199-215, https://doi.org/10.1016/j.jhydrol.2012.07.006.

Malcolm IA , Soulsby C, Youngson AF, Petry J (2003) Heterogeneity in ground water–surface water interactions in the hyporheic zone of a salmonid spawning stream. Hydrol. Process. 17, 601–617, DOI: 10.1002/hyp.1156

Malcolm IA , Soulsby C, Youngson AF, Hannah DM, McLaren IS, Thorne A (2004) Hydrological influences on hyporheic water quality: implications for salmon egg survival. Hydrol. Process. 18, 1543–1560, DOI: 10.1002/hyp.1405

Malenda HF, Sutfin NA, Guryan G, Stauffer S, Rowland JC, Williams KH, and Singha K (2019) From Grain to Floodplain: Evaluating heterogeneity of floodplain hydrostatigraphy using sedimentology, geophysics, and remote sensing. Earth Surf. Process. Landforms. DOI: 10.1002/esp.4613

Martone I, Gualtieri C, Endreny T (2020) Characterization of Hyporheic Exchange Drivers and Patterns within a Low-Gradient, First-Order, River Confluence during Low and High Flow. Water 2020, 12, 649, doi:10.3390/w12030649

Nelson AR, Sawyer AH, Gabor RS, Saup CM, Bryant SR, Harris KD, Briggs MA, Williams KH, Wilkins MJ (2019) Heterogeneity in hyporheic flow, pore water chemistry, and microbial community composition in an alpine streambed. J Geophys Res Biogeosci. DOI: 10.1029/2019JG005226

O'Connor BL, Harvey JW, and McPhillips LE (2012), Thresholds of flow-induced bed disturbances and their effects on stream metabolism in an agricultural river, Water Resour. Res., 48, W08504, doi:10.1029/2011WR011488.

Rau GC, Cuthbert MO, McCallum AM, Halloran LJS, and Andersen MS (2015), Assessing the accuracy of 1-D analytical heat tracing for estimating near-surface sediment thermal diffusivity and water

flux under transient conditions. J. Geophys. Res. Earth Surf., 120, 1551– 1573. doi: 10.1002/2015JF003466.

Sawyer AH, and Cardenas MB (2009), Hyporheic flow and residence time distributions in heterogeneous cross-bedded sediment, Water Resour. Res., 45, W08406, doi:10.1029/2008WR007632.

Soulsby CA, Youngson AF, Moir H, Malcolm I (2001). Fine sediment influence on salmonid spawning habitat in a lowland agricultural stream: A preliminary assessment. The Science of the total environment. 265. 295-307. 10.1016/S0048-9697(00)00672-0.

Stallman RW (1965), Steady one-dimensional fluid flow in a semi-infinite porous medium with sinusoidal surface temperature, J. Geophys. Res., 70(12), 2821– 2827, doi:10.1029/JZ070i012p02821.Taylor CJ, Pedregal DJ, Young PC, Tych W (2007) Environmental time series analysis and forecasting with the Captain toolbox, Environmental Modelling & Software, Volume 22, Issue 6, 2007, Pages 797-814, ISSN 1364-8152, https://doi.org/10.1016/j.envsoft.2006.03.002.

Tokunaga T, Carroll R, Conrad M, Tran A, Wan J, Williams K (2019): Hillslope subsurface flow and transport data for the PLM transect in East River, Colorado. Watershed Function SFA. doi:10.21952/WTR/1506941

Valett HM, Dahm CN, Campana ME, Morrice JA, Baker MA, Fellows CS (1997) Hydrologic Influences on Groundwater-Surface Water Ecotones: Heterogeneity in Nutrient Composition and Retention. J of the North American Benthological Society, Vol. 16, No. 1, pp.239-247. http://www.jstor.org/stable/1468254 .

Young PC, Pedregal D, and Tych W (1999). Dynamic harmonic regression. J. of Forecasting, 18, 369–394.

Appendix:

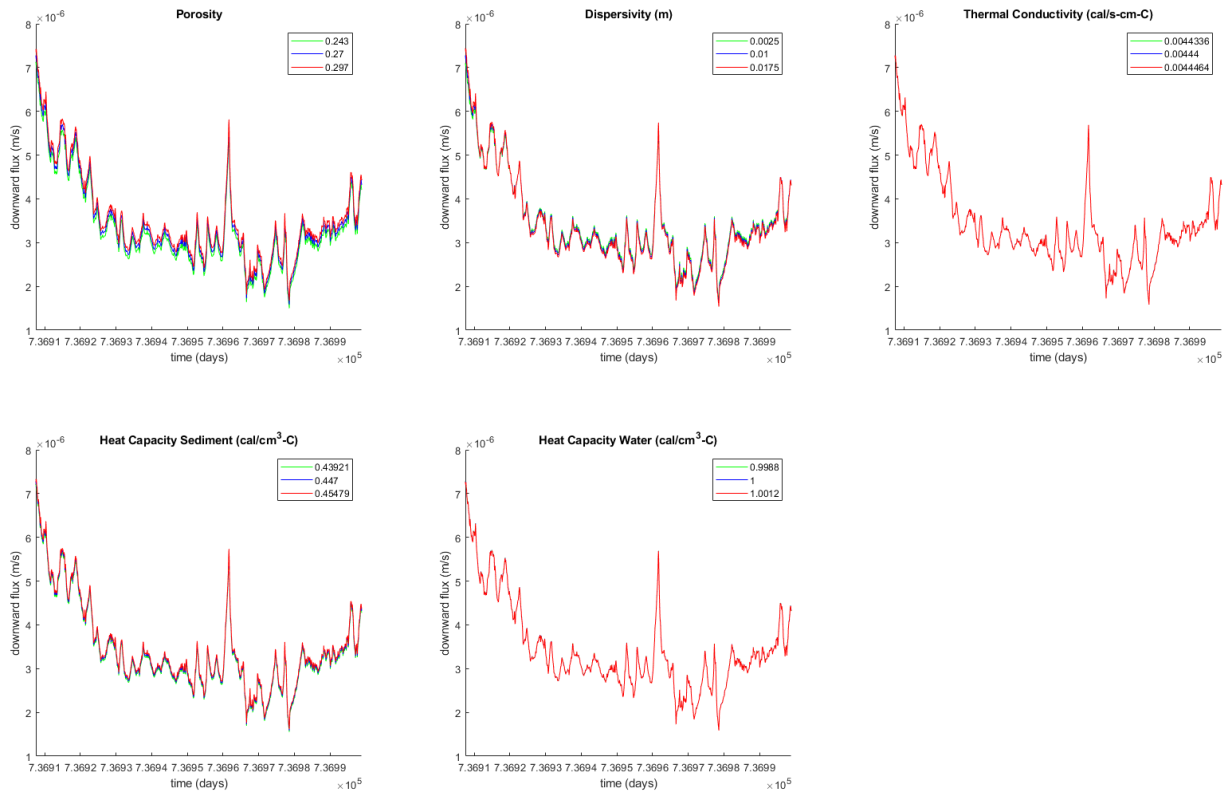

Figure A1: 2017 parameter sensitivity analysis for river to 10 cm depth with x-axis in days since January 1, 0000.

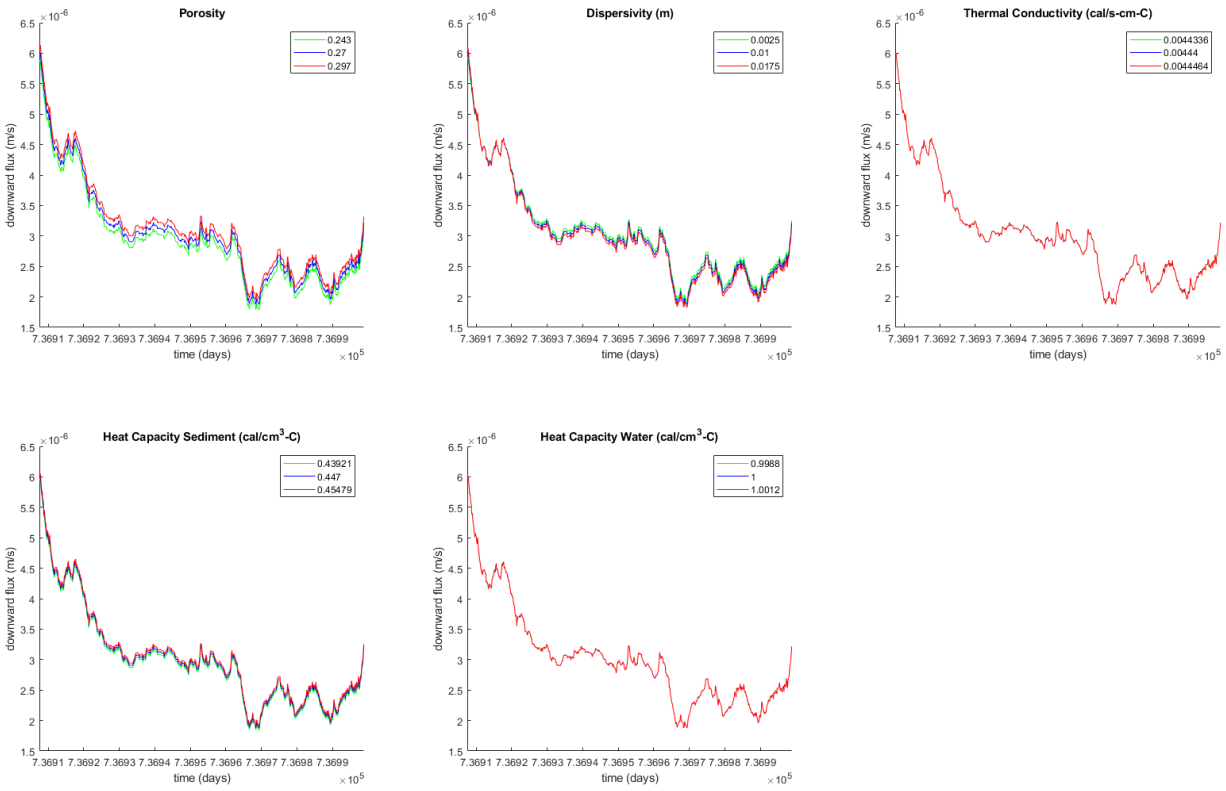

Figure A2: 2017 parameter sensitivity analysis for 10 cm to 20 cm depth with x-axis in days since January 1, 0000.

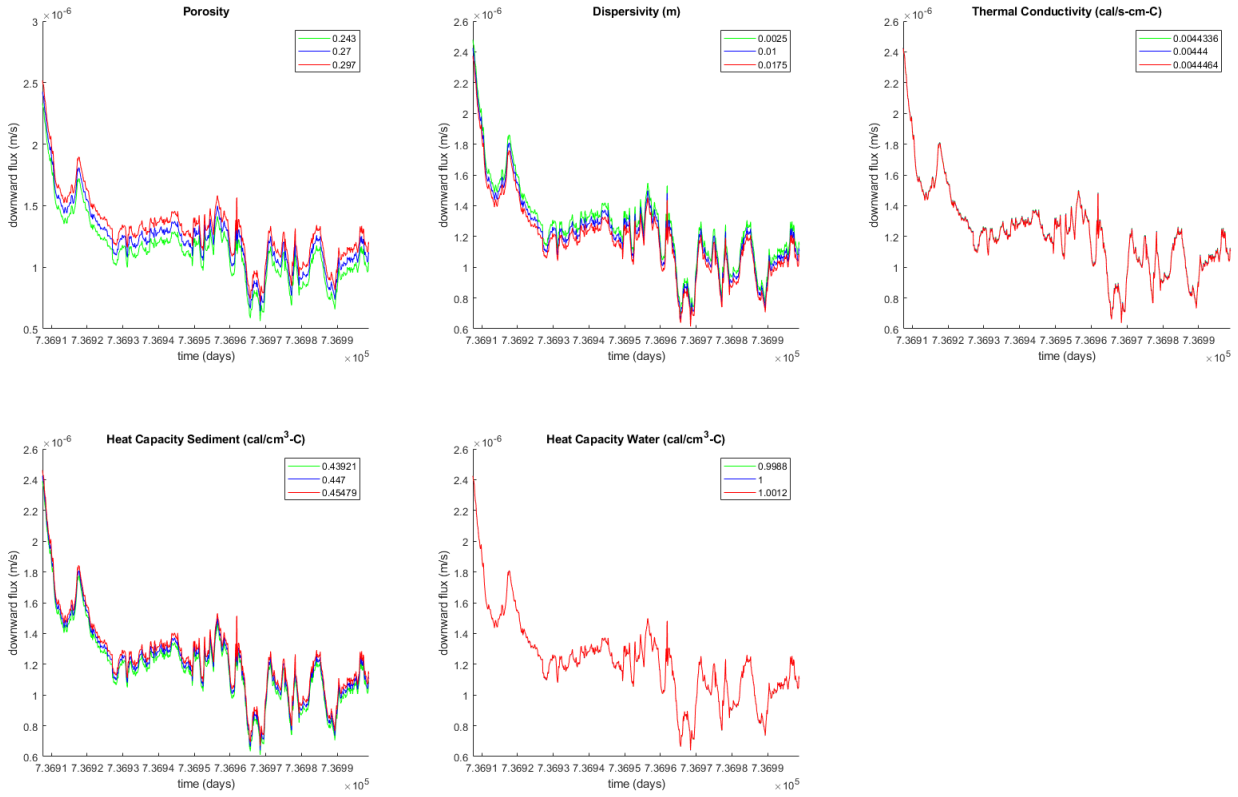

Figure A3: 2017 parameter sensitivity analysis for 20 cm to 35 cm depth with x-axis in days since January 1, 0000.

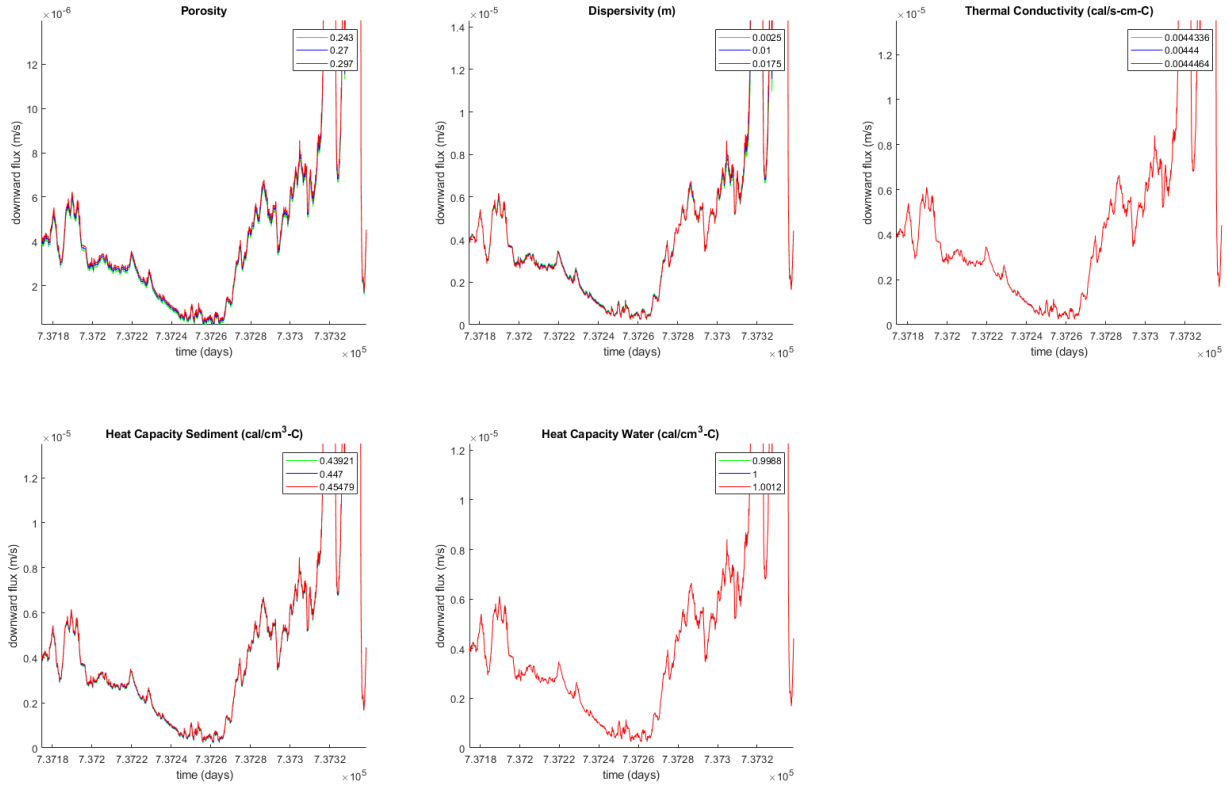

Figure A4: 2018 parameter sensitivity analysis for river to 10 cm depth with x-axis in days since January 1, 0000.

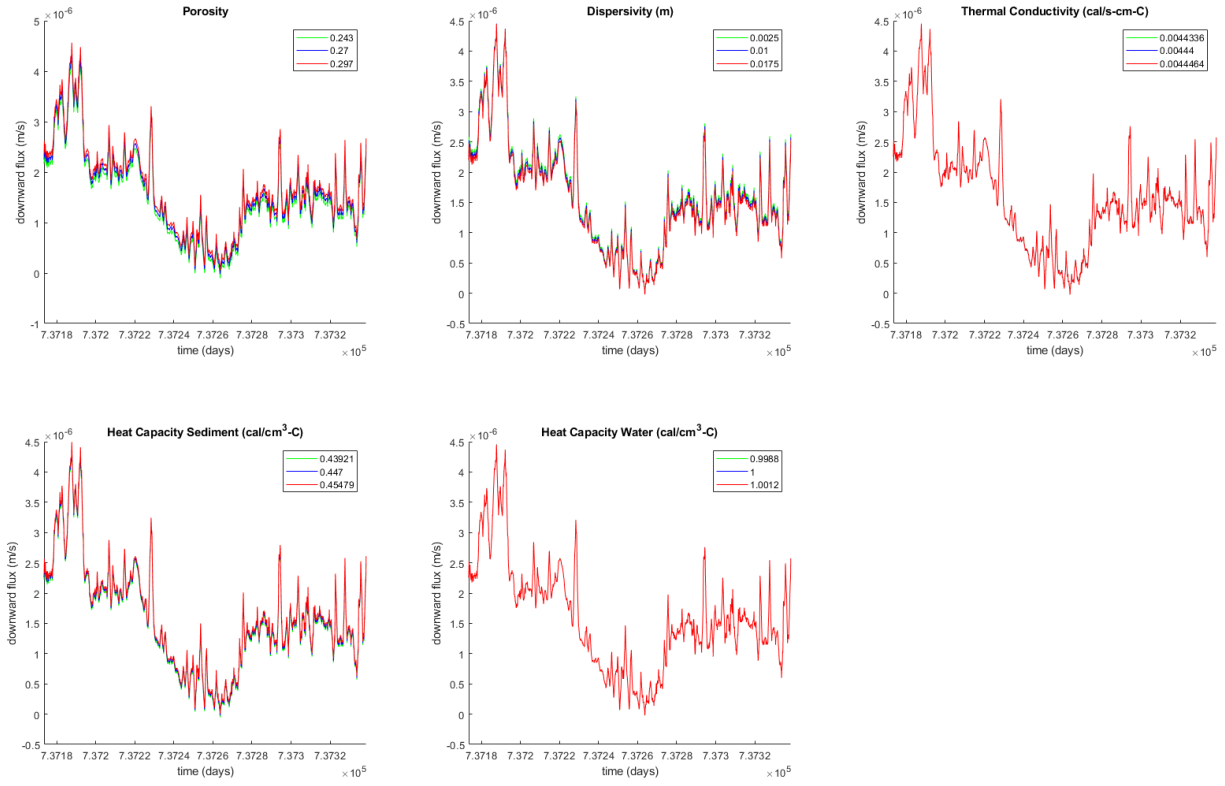

Figure A5: 2018 parameter sensitivity analysis for 10 cm to 20 cm depth with x-axis in days since January 1, 0000.

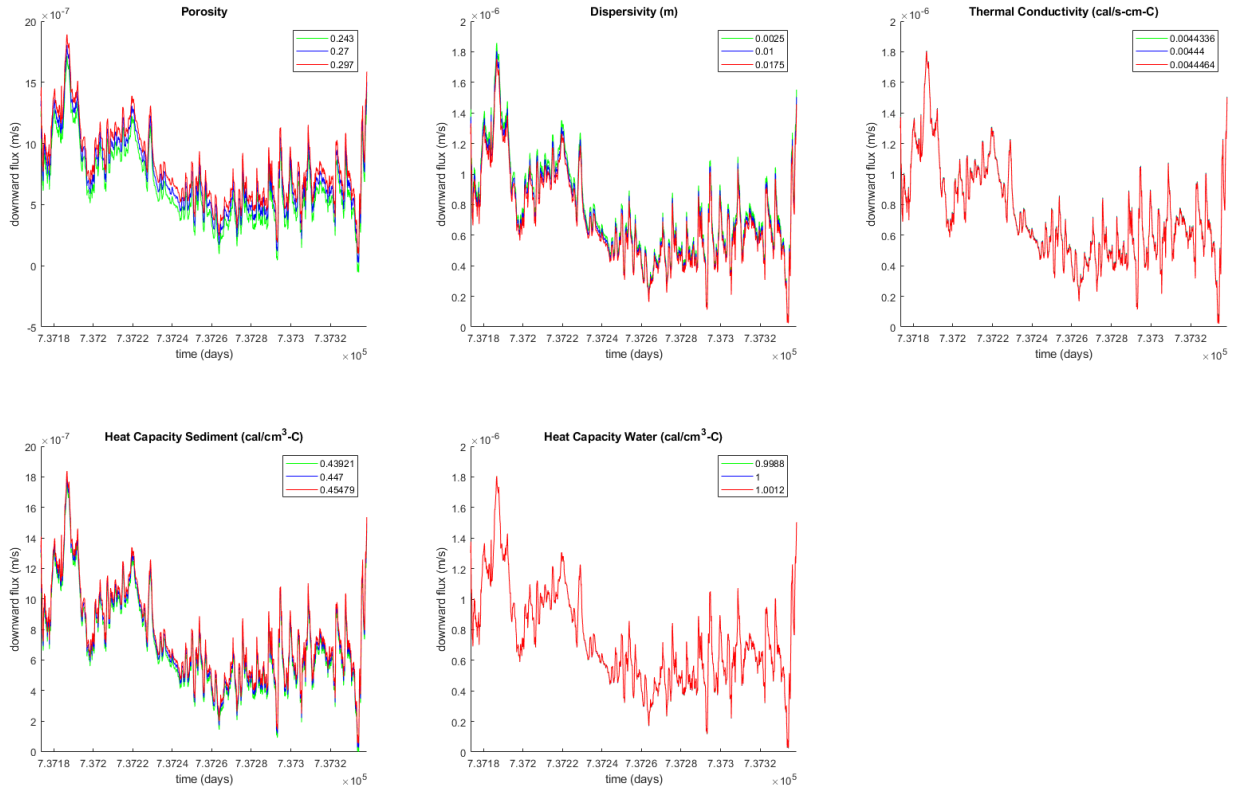

Figure A6: 2018 parameter sensitivity analysis for 20 cm to 35 cm depth with x-axis in days since January 1, 0000.